Kaon photoproduction: Data consistency, coupling constants, and polarization observables

R. A. Adelseck and B. Saghai
Département de Physique Nucléaire-Haute Energie, Centre d'Etudes Nucléaires de Saclay, 91191 Gif-sur-Yvette CEDEX, France
(Received 3 October 1989)

The process $\gamma p \to K^+\Lambda$ is studied in a phenomenological approach. A thorough analysis of the existing differential cross section data up to 1.4 GeV, taking into account the systematic uncertainties, shows the Orsay data to be internally inconsistent. Removing this data set from the data base results in a rather simple reaction mechanism with the extracted main kaon-hyperon-nucleon coupling constants in agreement with the SU(3) predictions. Employing a diagrammatic model, the differential and total cross section, Λ-polarization, and polarized target data are well reproduced. Predictions for other single and double polarization observables and suggestions for new measurements are presented. Applying crossing symmetry, the reaction is related to the radiative K^- capture process, and a comparison with the measured branching ratio is made.

I. INTRODUCTION

The main field of interest in intermediate-energy physics has been nucleon-nucleon interactions as well as the properties and the behavior of the first baryonic resonance, where at the subnucleonic level only u and d quarks are involved. The quantum number of strangeness brought about by the s quark introduces a new degree of freedom into this domain. It implies the investigation of hyperon-nucleon and hyperon-hyperon interactions, the production and propagation of strange hadronic resonances, and strangeness exchange mechanisms.

Reactions like (K^-,π^-) or (π^+,K^+), kaon-nucleon, and hyperon-nucleon scattering are the most common methods in the domain of strangeness physics, both experimentally and theoretically.[1] However, because of the strongly interacting nature of *both* the incident *and* the outgoing particles with the target nucleons, the extraction of quantitative information remains very model dependent.

An attractive alternative to hadronic processes is the use of electromagnetic probes.[2] In this procedure, distortions in the incident and outgoing channels are largely reduced due to the rather weakly interacting nature of both the photon and the K^+ with hadrons. The weakness of these interactions then justifies a first-order theoretical description of the reaction, but results in cross sections smaller than those of hadronic reactions.

The effort in understanding kaon photoproduction off the nucleon is expected to provide a convenient means in our knowledge of the fundamental kaon-hyperon-nucleon (KYN) coupling constants as well as the reaction mechanism. Besides, it serves as a first step in further studies of strangeness in hadronic aggregates.

After two decades of investigation, the field of electromagnetic production of strangeness had been dormant since the mid-1970s mainly due to a lack of adequate experimental facilities and a seemingly complicated elementary reaction mechanism. Recent theoretical studies of K^+ photoproduction and electroproduction[2] have been motivated by the new generation of accelerators, which will provide continuous, high-current, and polarized beams in the energy domain of a few GeV's; the threshold for the elementary reactions $\gamma p \to K^+\Lambda$ and $\gamma p \to K^+\Sigma^0$ being at 0.911 GeV and 1.046 GeV, respectively.

In this paper we concentrate on the kaon photoproduction process associated with the production of a lambda, i.e., the reaction

$$\gamma + p \to K^+ + \Lambda \ .$$

The second section is devoted to a discussion of the KYN coupling constants. Within a phenomenological approach we extract the relevant coupling constants by performing a least-squares search based on the available data. Following previous descriptions,[3,4] we derive the photoproduction operator based on a few selected first-order Feynman diagrams showing the importance of nucleon-, hyperon-, and kaon-exchange terms. Through crossing symmetry we relate the $\gamma p \to K^+\Lambda$ reaction to the radiative kaon capture process $K^- p \to \gamma\Lambda$ and calculate the branching ratio $\Gamma(K^- p \to \gamma\Lambda)/\Gamma(K^- p \to \text{all})$.

After a brief presentation of the formalism, we summarize the status of the experimental results from threshold up to 1.4 GeV. We show why and how a thorough analysis of the data leads us to the inclusion of not only the statistical uncertainties (as in all previous investigations) when fitting the differential cross section data, but also the systematic ones. This procedure allows us on one hand to clear up the old quest of inconsistencies within the experimental results, and on the other hand to show, for the first time, that the values of the two main coupling constants ($g_{K\Lambda N}$ and $g_{K\Sigma N}$) extracted from photoproduction reactions come out consistent with SU(3) predictions.

In the third section, we present a comprehensive study of the observables in the kaon photoproduction reaction (differential and total cross section, single and double polarization asymmetries) and in the radiative kaon capture

process (branching ratio) related to it via crossing. The crucial role of the polarization observables in our understanding of the reaction mechanism is emphasized.

In the fourth and last section we conclude, after a synthesis of our investigations, with suggestions about future experimental studies and possible theoretical improvements.

In order to keep the main body of this paper simple and to facilitate its reading, we have moved the SU(3) relations for the relevant couplings, the explicit expressions for the amplitudes derived from the Feynman diagrams, the vertex factors and propagators, and the complete table of data points and error bars (including systematic uncertainties) to several Appendixes.

II. DETERMINATION OF KAON-HYPERON-NUCLEON COUPLING CONSTANTS AND SU(3) PREDICTIONS

This section contains three subsections. In the first subsection, we elaborate on the current status of our knowledge of the $K\Lambda N$ and $K\Sigma N$ coupling constants, their phenomenologically determined values, as well as on their strengths as predicted by SU(3) symmetry.

In the second subsection, we outline the theoretical technique employed in the derivation of the invariant scattering amplitude for the $\gamma p \rightarrow K^+\Lambda$ reaction. We further establish the relation between the photoproduction process and radiative kaon capture to obtain an expression for the branching ratio $\Gamma(K^- p \rightarrow \gamma\Lambda)/\Gamma(K^- p \rightarrow \text{all})$.

In the third subsection, we analyze the available data under the point of view of internal and external consistencies. Within a phenomenological approach we discuss the existing experimental results and give a table of coupling constants as obtained from a least-squares fit to the data.

A. Kaon-hyperon-nucleon coupling constants

The kaon-hyperon-nucleon coupling constants (g_{KYN}), hereafter referred to as KYN CC's, have been investigated for almost three decades. Nevertheless, the determination of even the two main couplings ($g_{K\Lambda N}$ and $g_{K\Sigma N}$) still remains problematic.

The knowledge of these fundamental quantities is indispensable in our understanding of the interaction of strange particles with nucleons. An attractive feature of this problem is due to the fact that SU(3) symmetry yields definite predictions[5] for these couplings in terms of the rather accurately known πNN coupling constant (see Appendix A). Starting from experimental results, the extraction of the KYN CC's is mainly performed by fitting either the kaon-nucleon scattering data or the measured differential cross section of the reaction $\gamma p \rightarrow K^+\Lambda$.

In this subsection, we show that the commonly agreed upon conclusion according to which the electromagnetic production of kaons leads to KYN CC values in disagreement with SU(3) predictions and hadronic reaction results is *not correct*. A careful and detailed study of all relevant experimental and theoretical investigations allows us not only to remedy these longstanding discrepancies, but also to shed light on the origins of the unrealistic values obtained in previous works for more than twenty years. In Table I, the most recent results for the two main coupling constants are shown including their SU(3) predictions.

The study of kaon-nucleon interactions seems to be a natural approach to the determination of the KYN CC's. The application of dispersion relation techniques[6] to strong interactions is known to allow the determination of pion-nucleon coupling constants from the measured scattering cross sections. The use of this tool for the KN process, however, has been less fruitful. Even a short discussion of the major problems encountered in this realm would be out of the scope of this paper. We refer the interested reader to condensed[2,7] or detailed[8] reviews.

In Table I, we report the results of two recent analyses[9,10] of kaon-nucleon scattering data aimed to determine the KYN CC's. We remark that while the absolute values for $g_{K\Lambda N}$ are in good agreement with SU(3) predictions, those for $g_{K\Sigma N}$ are too large. Notice that the relative sign of the coupling constants is not determined, since from hadronic interactions only the squares of KYN CC's are extracted.

Bozoian *et al.*[11] obtain good results for the KYN CC's by introducing a quark pairing mechanism as a possible scheme of boson exchange processes in hyperon-nucleon potential models.[12] Values coming from the investigation of kaon photoproduction and/or electroproduction[3,4,13–17] are widely scattered and in disagreement with the expected results. The reasons for this situation are discussed in Sec. II C.

B. Theoretical formalism

The methods used in the theoretical investigation of kaon photoproduction below 2 GeV can be classified into three categories (disregarding studies based on Regge pole methods[18] or parton-quark approaches,[19] both concerning higher-energy domains): (a) dispersion relations,[20] (b) multipole analyses,[21] and (c) isobaric models.[13,14] Problems related to these methods have been discussed elsewhere.[7,22]

Using an isobaric model, we construct a Lorentz-invariant operator by applying a diagrammatic technique. In this approach, the Born terms and the contributions from the excitation of intermediate resonant states, above as well as below threshold, are represented by lowest-order Feynman diagrams (Fig. 1). From Fig. 1 it is clear that in terms of their mathematical properties as well as of their physical meaning there exist three distinct structures contributing to the reaction mechanism. The direct s-channel represents the propagation of a nucleonic state, while the u and t channels account for the exchange of the hyperonic and kaonic resonances, respectively. Due to our use of a relativistic formalism,[23] the time-ordered forward and backward (particle and antiparticle) propagation of the intermediate state are taken into account in a natural way.

In our study, we investigate the effects of all known[24] spin-$\frac{1}{2}$ and spin-$\frac{3}{2}$ nucleonic resonances, the contributions

TABLE I. $K\Lambda N$ and $K\Sigma N$ coupling constants.

Source	$g_{K\Lambda N}/\sqrt{4\pi}$	$g_{K\Sigma N}/\sqrt{4\pi}$	Reference (year)
SU(3)	$-4.4 \div -3.0$	$+0.9 \div +1.3$	See Appendix A
K-N scattering	3.73[a]	<1.82[a]	Martin (Ref. 9) (1981)
K-N scattering	3.53[a]	1.53[a]	Antolin (Ref. 10) (1986)
Y-N scattering	-4.13	$+0.82$	Bozoian *et al.* (Ref. 11) (1983)
$p(\gamma,K^+)\Lambda$	$-2.6 \div -1.1$	$-0.9 \div +1.0$	Thom (Ref. 13) (1966)
$p(\gamma,K^+)\Lambda$	-2.4	$+0.4$	Renard and Renard (Ref. 14) (1971/1972)
$p(\gamma,K^+)\Sigma^0$	-3.6	$+0.6$	
$p(\gamma,K^+)\Lambda$	-1.29	$+1.97$	Adelseck *et al.* (Ref. 3) (1985)
$p(\gamma,K^+)\Lambda$	-4.30	-1.84	Adelseck and Wright (Ref. 4) (1988)
$p(\gamma,K^+)\Lambda$	-2.90	-3.44	
$p(\gamma,K^+)\Lambda$ and $p(e,e'K^+)\Lambda$	-3.15	-1.68	
$p(\gamma,K^+)\Lambda$	-0.91	$+0.62$	Rosenthal *et al.* (Ref. 15) (1988)
$p(\gamma,K^+)\Sigma^0$	-1.84	$+2.72$	Bennhold (Ref. 16) (1989)
$p(\gamma,K^+)\Lambda$	-2.0	-0.8	Cohen (Ref. 17) (1989)
$p(\gamma,K^+)\Lambda$	-4.17	$+1.18$	Present work

[a]Sign undetermined.

of all known spin-$\frac{1}{2}$ lambda and sigma resonances, and the influences of the two lowest-lying kaon resonances, i.e., the vector-kaon state $K^*(892)$ and the pseudovector state $K1(1280)$. The physical values of all the particles considered are given in Table V (Appendix B).

The Mandelstam variables s, t, and u, corresponding to Fig. 1 parts (a), (f), and (g), parts (b), (e), and (e'), and parts (c), (d), and (h) are defined by

$$s=(p_p+p_\gamma)^2,\quad t=(p_\gamma-p_K)^2,\quad u=(p_p-p_K)^2\ , \tag{1}$$

respectively, where $p_\gamma=(E_\gamma,\mathbf{p}_\gamma)$, p_p, p_K, and p_Λ are the four-vectors of the photon, proton, kaon, and lambda, respectively. To obtain a convenient expression for the scattering amplitude, we recall that the $\mathcal{S}$ matrix for the photoproduction of pseudoscalar mesons can be written in the form

$$\mathcal{S}_{fi}=\frac{1}{(2\pi)^2}\left[\frac{M_pM_\Lambda}{4E_\Lambda E_K E_p E_\gamma}\right]^{1/2}\mathcal{M}_{fi} \times\delta^{(4)}(p_p+p_\gamma-p_K-p_\Lambda)\ , \tag{2}$$

with the Lorentz-invariant matrix element $\mathcal{M}_{fi}$ being given by

$$\mathcal{M}_{fi}=\bar{u}(\mathbf{p}_\Lambda,s_\Lambda)\sum_{j=1}^{4}\mathcal{A}_j\mathcal{M}_j u(\mathbf{p}_p,s_p) \tag{3}$$

and

$$\mathcal{M}_1=-\gamma_5\gamma\cdot\varepsilon\gamma\cdot p_\gamma\ , \tag{4a}$$

$$\mathcal{M}_2=2\gamma_5(\varepsilon\cdot p_p p_\gamma\cdot p_\Lambda-\varepsilon\cdot p_\Lambda p_\gamma\cdot p_p)\ , \tag{4b}$$

$$\mathcal{M}_3=\gamma_5(\gamma\cdot\varepsilon p_\gamma\cdot p_p-\gamma\cdot p_\gamma\varepsilon\cdot p_p)\ , \tag{4c}$$

$$\mathcal{M}_4=\gamma_5(\gamma\cdot\varepsilon p_\gamma\cdot p_\Lambda-\gamma\cdot p_\gamma\varepsilon\cdot p_\Lambda)\ . \tag{4d}$$

The explicit expressions for the contributions of each state and channel to the amplitudes $\mathcal{A}_j$ are tabulated in Appendix B.

We obtain an alternative representation often used in the description of the amplitude by expressing Eq. (3) in terms of two-component spinors χ. In the c.m. frame, the matrix element $\mathcal{M}_{fi}$ can then be written as

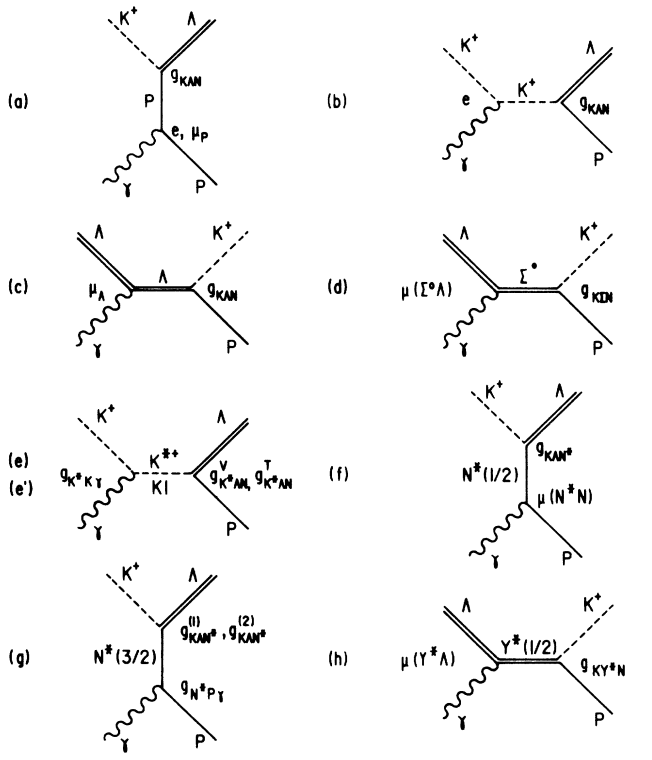

FIG. 1. Feynman diagrams for the process $\gamma p\rightarrow K^+\Lambda$. (a)–(c) show the Born terms, (d) stands for the Σ^0 exchange, (e) and (e') represent the spin-1 kaon resonances K^{*+} and $K1$, (f) and (g) correspond to the spin-$\frac{1}{2}$ and spin-$\frac{3}{2}$ resonances, and (h) represents the spin-$\frac{1}{2}$ hyperon resonances.

$$\mathcal{M}_{fi}=\left[\frac{E_\Lambda+M_\Lambda}{2M_\Lambda}\right]^{1/2}\left[\frac{E_p+M_p}{2M_p}\right]^{1/2}\langle\chi(\Lambda)|\mathcal{F}|\chi(p)\rangle\ , \tag{5}$$

where

$$\mathcal{F}=\boldsymbol{\sigma}\cdot\hat{\boldsymbol{\epsilon}}\mathcal{F}_1+i(\boldsymbol{\sigma}\cdot\hat{\mathbf{p}}_K)(\boldsymbol{\sigma}\cdot\hat{\mathbf{p}}_\gamma\times\hat{\boldsymbol{\epsilon}})\mathcal{F}_2 +(\boldsymbol{\sigma}\cdot\hat{\mathbf{p}}_\gamma)(\hat{\mathbf{p}}_K\cdot\hat{\boldsymbol{\epsilon}})\mathcal{F}_3+(\boldsymbol{\sigma}\cdot\hat{\mathbf{p}}_K)(\hat{\mathbf{p}}_K\cdot\hat{\boldsymbol{\epsilon}})\mathcal{F}_4\ , \tag{6}$$

and the $\mathcal{F}_j$ are the Chew, Goldberger, Low, and Nambu (CGLN) amplitudes.[25] Their relation to the amplitudes $\mathcal{A}_j$ is given by[13]

$$\mathcal{F}_1=-(\sqrt{s}-M_\Lambda)\mathcal{A}_1+p_\gamma\cdot p_p\mathcal{A}_3+p_\gamma\cdot p_\Lambda\mathcal{A}_4\ , \tag{7a}$$

$$\mathcal{F}_2=\frac{|\mathbf{p}_\gamma||\mathbf{p}_K|}{(E_p+M_p)(E_\Lambda+M_\Lambda)}[(\sqrt{s}+M_\Lambda)\mathcal{A}_1+p_\gamma\cdot p_p\mathcal{A}_3 +p_\gamma\cdot p_\Lambda\mathcal{A}_4]\ , \tag{7b}$$

$$\mathcal{F}_3=\frac{|\mathbf{p}_\gamma||\mathbf{p}_K|}{(E_\Lambda+M_\Lambda)}[2p_\gamma\cdot p_\Lambda\mathcal{A}_2-(\sqrt{s}+M_\Lambda)\mathcal{A}_3]\ , \tag{7c}$$

$$\mathcal{F}_4=-\frac{|\mathbf{p}_K|^2}{(E_p+M_p)}[2p_\gamma\cdot p_\Lambda\mathcal{A}_2+(\sqrt{s}-M_\Lambda)\mathcal{A}_3]\ . \tag{7d}$$

The general expression of the differential cross section has the form

$$d\sigma=(2\pi)^4\frac{M_pM_\Lambda|\mathcal{M}_{fi}|^2\delta^{(4)}(p_p+p_\gamma-p_K-p_\Lambda)}{4E_\Lambda E_K[(p_p\cdot p_\gamma)^2-p_p^2\cdot p_\gamma^2]^{1/2}} \times\frac{d^3p_Kd^3p_\Lambda}{(2\pi)^6}\ , \tag{8}$$

which in the c.m. frame reduces to

$$d\sigma^{\text{c.m.}}=\frac{(E_p+M_p)(E_\Lambda+M_\Lambda)}{64\pi^2s}\frac{|\mathbf{p}_K|}{2|\mathbf{p}_\gamma|}\,\mathrm{Tr}(\mathcal{F}^\dagger\mathcal{F})\ . \tag{9}$$

The advantage of a formalism using CGLN amplitudes lies in the fact that they can easily be subject to a multipole analysis. To study polarization observables, however, we will choose a more convenient representation employing transversity amplitudes,[26,27] denoted by b_j. They are obtained by using a reference frame in which the proton and lambda have well-defined spin projections with respect to the y axis,

$$\hat{y}=\frac{\mathbf{p}_\gamma\times\mathbf{p}_K}{|\mathbf{p}_\gamma\times\mathbf{p}_K|}\ .$$

Denoting the c.m. angle between the incoming photon and the outgoing kaon by θ, we define the transversity amplitudes in terms of the CGLN amplitudes:

$$b_1=-\frac{i}{\sqrt{2}}(\mathcal{F}_1-\mathcal{F}_2e^{-i\theta})e^{i\theta/2}\ , \tag{10a}$$

$$b_2=\frac{i}{\sqrt{2}}(\mathcal{F}_1-\mathcal{F}_2e^{i\theta})e^{-i\theta/2}\ , \tag{10b}$$

$$b_3=-b_1-\frac{\sin\theta}{\sqrt{2}}(\mathcal{F}_3+\mathcal{F}_4e^{-i\theta})e^{i\theta/2}\ , \tag{10c}$$

$$b_4=-b_2-\frac{\sin\theta}{\sqrt{2}}(\mathcal{F}_3+\mathcal{F}_4e^{i\theta})e^{-i\theta/2}\ . \tag{10d}$$

Since the photoproduction process is described by four complex amplitudes [Eqs. (3), (7), or (10)] $b_j=b_{j1}+ib_{j2}$, $j=1,\ldots,4$, we can form 16 real bilinear forms $b_{ik}b_{j\ell}$, $i,j=1,\ldots,4$, $k,\ell=1,2$, i.e., there are 16 observables which can be used to determine the reaction amplitude[28] (Table II).

The lambda polarization asymmetry P, polarized photon asymmetry Σ, and polarized target asymmetry T are defined by

$$P=\frac{d\sigma/d\Omega^{(+)}-d\sigma/d\Omega^{(-)}}{d\sigma/d\Omega^{(+)}+d\sigma/d\Omega^{(-)}}\ , \tag{11}$$

$$\Sigma=\frac{d\sigma/d\Omega^{(\perp)}-d\sigma/d\Omega^{(\parallel)}}{d\sigma/d\Omega^{(\perp)}+d\sigma/d\Omega^{(\parallel)}}\ , \tag{12}$$

$$T=\frac{d\sigma/d\Omega^{(+)}-d\sigma/d\Omega^{(-)}}{d\sigma/d\Omega^{(+)}+d\sigma/d\Omega^{(-)}}\ , \tag{13}$$

respectively, where + (−) refers to a hadron polarized parallel (antiparallel) to the y axis, and ⊥ (∥) to a photon linearly polarized perpendicular (parallel) to the reaction plane. The definition of the double polarization asymmetry parameters is given by[29]

$$X=\frac{d\sigma/d\Omega^{(++)}+d\sigma/d\Omega^{(--)}-d\sigma/d\Omega^{(+-)}-d\sigma/d\Omega^{(-+)}}{d\sigma/d\Omega^{(++)}+d\sigma/d\Omega^{(--)}+d\sigma/d\Omega^{(+-)}+d\sigma/d\Omega^{(-+)}}\ , \tag{14}$$

with X denoting any one of the 12 double polarization observables, numbered 5–16 (Table II), and + (−) denoting a polarization parallel (antiparallel) to the respective quantization axis as specified in Table II. In the case of a circularly polarized photon beam, + (−) is equivalent to the helicity state +1 (−1), while in the case of the linearly polarized (t) photon beam it refers to a state with the polarization vector forming an angle of 45° (−45°) with the x axis. Note that the particular choice of the quantization axes in Table II allows us to rewrite Eq. (14):

$$X=\frac{d\sigma/d\Omega^{(++)}-d\sigma/d\Omega^{(+-)}}{d\sigma/d\Omega^{(++)}+d\sigma/d\Omega^{(+-)}} =\frac{d\sigma/d\Omega^{(--)}-d\sigma/d\Omega^{(-+)}}{d\sigma/d\Omega^{(--)}+d\sigma/d\Omega^{(-+)}}\ , \tag{15}$$

due to the equivalence $d\sigma/d\Omega^{(++)}=d\sigma/d\Omega^{(--)}$ and $d\sigma/d\Omega^{(+-)}=d\sigma/d\Omega^{(-+)}$.

It is important to notice that the 16 observables are not independent. The redundancy in the observables is reflected by the following nonlinear relations:

TABLE II. Observables in pseudoscalar meson photoproduction. $\mathcal{N}$ includes flux and normalization factors, and is given by $(E_p+M_p)(E_\Lambda+M_\Lambda)|\mathbf{p}_K|/64\pi^2 s 2|\mathbf{p}_\gamma|$.

Observable	Polarization[a] of γ	p	Λ	
1. $\{d\sigma/d\Omega\}/\mathcal{N}$				$=\|b_1\|^2+\|b_2\|^2+\|b_3\|^2+\|b_4\|^2$
Single polarization				
2. $P\cdot\{d\sigma/d\Omega\}/\mathcal{N}$			y'	$=\|b_1\|^2-\|b_2\|^2+\|b_3\|^2-\|b_4\|^2$
3. $\Sigma\cdot\{d\sigma/d\Omega\}/\mathcal{N}$	p			$=\|b_1\|^2+\|b_2\|^2-\|b_3\|^2-\|b_4\|^2$
4. $T\cdot\{d\sigma/d\Omega\}/\mathcal{N}$		y		$=\|b_1\|^2-\|b_2\|^2-\|b_3\|^2+\|b_4\|^2$
Double polarizaton				
Beam-target				
5. $E\cdot\{d\sigma/d\Omega\}/\mathcal{N}$	c	z		$=2\,\mathrm{Re}(b_1 b_3^*+b_2 b_4^*)$
6. $F\cdot\{d\sigma/d\Omega\}/\mathcal{N}$	c	x		$=2\,\mathrm{Im}(b_1 b_3^*-b_2 b_4^*)$
7. $G\cdot\{d\sigma/d\Omega\}/\mathcal{N}$	t	z		$=2\,\mathrm{Im}(b_1 b_3^*+b_2 b_4^*)$
8. $H\cdot\{d\sigma/d\Omega\}/\mathcal{N}$	t	x		$=-2\,\mathrm{Re}(b_1 b_3^*+b_2 b_4^*)$
Beam-recoil				
9. $C_x\cdot\{d\sigma/d\Omega\}/\mathcal{N}$	c		x'	$=-2\,\mathrm{Im}(b_1 b_4^*-b_2 b_3^*)$
10. $C_y\cdot\{d\sigma/d\Omega\}/\mathcal{N}$	c		z'	$=2\,\mathrm{Re}(b_1 b_4^*+b_2 b_3^*)$
11. $O_x\cdot\{d\sigma/d\Omega\}/\mathcal{N}$	t		x'	$=2\,\mathrm{Re}(b_1 b_4^*-b_2 b_3^*)$
12. $O_z\cdot\{d\sigma/d\Omega\}/\mathcal{N}$	t		z'	$=2\,\mathrm{Im}(b_1 b_4^*+b_2 b_3^*)$
Target-recoil				
13. $T_x\cdot\{d\sigma/d\Omega\}/\mathcal{N}$		x	x'	$=2\,\mathrm{Re}(b_1 b_2^*-b_3 b_4^*)$
14. $T_z\cdot\{d\sigma/d\Omega\}/\mathcal{N}$		x	z'	$=2\,\mathrm{Im}(b_1 b_2^*-b_3 b_4^*)$
15. $L_x\cdot\{d\sigma/d\Omega\}/\mathcal{N}$		z	x'	$=-2\,\mathrm{Im}(b_1 b_2^*+b_3 b_4^*)$
16. $L_z\cdot\{d\sigma/d\Omega\}/\mathcal{N}$		z	z'	$=2\,\mathrm{Re}(b_1 b_2^*+b_3 b_4^*)$

[a]Quantization axes are defined as follows: $\hat{z}=\hat{p}_p$, $\hat{y}=\mathbf{p}_\gamma\times\mathbf{p}_K/|\mathbf{p}_\gamma\times\mathbf{p}_K|$, $\hat{x}=\hat{y}\times\hat{z}$, $\hat{z}'=\hat{p}_\Lambda$, $\hat{y}'=\hat{y}$, $\hat{x}'=\hat{y}'\times\hat{z}'$. p—linearly polarized photon (0, $\pi/2$ with respect to scattering plane); t—linearly polarized photon ($\pm\pi/4$ with respect to scattering plane); c—circularly polarized photon.

$$E^2+F^2+G^2+H^2=1+P^2-\Sigma^2-T^2\ , \tag{16a}$$

$$FG-EH=P-\Sigma T\ , \tag{16b}$$

$$C_x^2+C_z^2+O_x^2+O_z^2=1+T^2-P^2-\Sigma^2\ , \tag{16c}$$

$$C_z O_x-C_x O_z=T-P\Sigma\ , \tag{16d}$$

$$T_x^2+T_z^2+L_x^2+L_z^2=1+\Sigma^2-P^2-T^2\ , \tag{16e}$$

$$T_x L_z-T_z L_x=\Sigma-PT\ . \tag{16f}$$

In addition, various inequalities can be derived[28,30] which impose more or less strong bounds on certain observables in terms of the numerical values of other observables.

Taking into account one arbitrary overall phase, we obtain complete information on the four complex amplitudes and the reaction mechanism by the knowledge of seven real quantities. Thus, given the differential cross section and the three single polarization observables, there is still need for three more measurements involving double polarization observables in order to determine the amplitude. Due to the relations (16), these measurements must not all be chosen from the same set (beam-target, beam-recoil, or recoil-target). At least one of the experiments must be performed on a different set. The sufficiency of this condition has been shown by Baker *et al.*[28] They also demonstrated that these seven measurements permit the determination of the scattering amplitude only up to quadrant ambiguities, i.e., up to certain phase factors. This is a consequence of the nonlinear structure of Eqs. (16). To resolve these ambiguities, two more experiments are required. Out of the needed five double polarization measurements Baker *et al.*[28] showed that no four must come from the same set. In summary, to determine unambiguously the four amplitudes b_i, or equivalently $\mathcal{A}_i$, we need to measure nine out of 16 observables.

To be exhaustive, we end our theoretical treatise on the observables by presenting the most general expression for the differential cross section involving any possible polarization of the photon beam, proton target, and recoiling lambda. We introduce the following notation: $\mathcal{P}_\gamma$ denotes the degree of right circular polarization (helicity state $+1$) of the photon beam, while P_γ describes the degree of linear polarization along an axis

$$\hat{n}=\hat{x}\cos\varphi+\hat{y}\sin\varphi\ .$$

The degree of the proton's polarization with respect to the x, y, and z axis is represented by P_x, P_y, and P_z, respectively. In this notation, the density matrices for the photon (in the helicity representation) and the proton are

given by

$$\rho_\gamma=\frac{1}{2}\begin{pmatrix}1+\mathcal{P}_\gamma & -P_\gamma\exp(-2i\varphi)\\ -P_\gamma\exp(2i\varphi) & 1-\mathcal{P}_\gamma\end{pmatrix}, \tag{17}$$

$$\rho_p=\tfrac{1}{2}(\mathbf{1}+\boldsymbol{\sigma}\cdot\mathbf{P}_p)=\frac{1}{2}\begin{pmatrix}1+P_z & P_x-iP_y\\ P_x+iP_y & 1-P_z\end{pmatrix}. \tag{18}$$

The density matrix for the lambda final state can be written analogously to Eq. (18) as

$$\rho_f=\tfrac{1}{2}(\mathbf{1}+\boldsymbol{\sigma}\cdot\mathbf{P}_f)\ .$$

We now have all the ingredients to present the expression for the differential cross section.

$$\begin{aligned}\rho_f\frac{d\sigma}{d\Omega}=\frac{1}{2}\left[\frac{d\sigma}{d\Omega}\right]_{\text{unpol}}\{&1-P_\gamma\Sigma\cos2\varphi+P_x(\mathcal{P}_\gamma F+P_\gamma H\sin2\varphi)+P_y(T-P_\gamma P\cos2\varphi)+P_z(\mathcal{P}_\gamma E+P_\gamma G\sin2\varphi)\\&+\sigma_{x'}[\mathcal{P}_\gamma C_x+P_\gamma O_x\sin2\varphi+P_x(T_x-P_\gamma L_z\cos2\varphi)+P_y(P_\gamma C_z\sin2\varphi-\mathcal{P}_\gamma O_z)\\&\quad+P_z(L_x+P_\gamma T_z\cos2\varphi)]\\&+\sigma_{y'}[P-P_\gamma T\cos2\varphi+P_x(\mathcal{P}_\gamma G-P_\gamma E\sin2\varphi)+P_y(\Sigma-P_\gamma\cos2\varphi)+P_z(P_\gamma F\sin2\varphi-\mathcal{P}_\gamma H)]\\&+\sigma_{z'}[\mathcal{P}_\gamma C_z+P_\gamma O_z\sin2\varphi+P_x(T_z+P_\gamma L_x\cos2\varphi)+P_y(-P_\gamma C_x\sin2\varphi+\mathcal{P}_\gamma O_z)\\&\quad+P_z(L_z-P_\gamma T_x\cos2\varphi)]\}\ .\end{aligned} \tag{19}$$

The matrices $\sigma_{x'}$, $\sigma_{y'}$, and $\sigma_{z'}$ refer to the lambda quantization axes as defined in Table II. From Eq. (19) we obtain the differential cross section for an outgoing lambda with an arbitrary quantization axis $\hat{n}'$ by taking the following trace:

$$\mathbf{P}_\Lambda\cdot\hat{n}'\frac{d\sigma}{d\Omega}=\mathrm{Tr}\left[\boldsymbol{\sigma}\cdot\hat{n}'\rho_f\frac{d\sigma}{d\Omega}\right]. \tag{20}$$

If the lambda's polarization is not observed, the expression for the differential cross section reduces to

$$\frac{d\sigma}{d\Omega}=\mathrm{Tr}\left[\rho_f\frac{d\sigma}{d\Omega}\right]. \tag{21}$$

Finally, we present the connection of the amplitudes for the kaon photoproduction mechanism $\gamma p\to K^+\Lambda$ to the radiative kaon capture process $K^-p\to\gamma\Lambda$. As has been pointed out by other authors,[31,32] these two reactions are related via crossing symmetry and, thus, are described by the same coupling constants. The close relation between these two mechanisms may then be used to obtain further insight into the involved couplings.

The relation between the amplitudes for the photoproduction process and the capture reaction can be found in the literature.[31] We will therefore only give a brief outline of the principle, based on intuitive arguments.

The general structure of the $\mathcal{S}$ matrix element in plane-wave Born approximation (PWBA) is given by

$$\begin{aligned}\mathcal{S}_{fi}\propto\int d^4x\,d^4y\,e^{-i(p_p+p_\gamma)\cdot x}e^{i(p_K+p_\Lambda)\cdot y}\\ \times\bar{u}(\Lambda)C_1S_FC_2u(p)\ ,\end{aligned} \tag{22}$$

where C_1 and C_2 are the appropriate vertex factors and S_F is the propagator of the intermediate state. Applying crossing changes—apart from flux and phase space factors—the plane wave factors to

$$e^{-i(p_p-p_\gamma)\cdot x}e^{i(-p_K+p_\Lambda)\cdot y}\ . \tag{23}$$

Note that this is not equivalent to an interchange of p_γ and p_K in Eq. (22), since such a substitution would result in a change of the vertex factors and propagators, as well.

Due to Eq. (23), the s (u) channel in the photoproduction amplitude will turn into a u- (s-) channel amplitude in the capture reaction. Furthermore, the photon (kaon) momentum operators will produce a $-p_\gamma$ ($-p_K$). Thus, we obtain the crossed amplitudes by inverting the sign of p_γ and p_K, and by interchanging the Mandelstam variables s and u. For a rigorous treatment we refer the reader to the article of Ji and Cotanch.[31]

The branching ratio for the radiative capture of kaons at rest,[33,34] defined by

$$\frac{\Gamma(K^-p\to\Lambda\gamma)}{\Gamma(K^-p\to\text{all})}\ ,$$

is independent of the kaon wave function, and is given by[32,35]

$$\frac{\Gamma(K^-p\to\Lambda\gamma)}{\Gamma(K^-p\to\text{all})}=\frac{M_\Lambda E_\gamma^{\text{c.m.}}}{8\pi W_p(M_p+M_K)M_K}\frac{1}{2}\sum_{\epsilon,s_p,s_\Lambda}|\tilde{\mathcal{M}}_{fi}|^2\ . \tag{24}$$

Here, $W_p=560\pm135$ MeV fm^3 is the imaginary part of the K^-p pseudopotential.[34] The matrix element for the capture reaction, $\tilde{\mathcal{M}}_{fi}$, is related to $\mathcal{M}_{fi}$ [Eq. (3)] via crossing symmetry.

C. Experimental situation and data fitting procedure

In the photoproduction operator derived in Sec. II B, the coupling constants at each vertex are treated as free parameters (except for the proton's and the lambda's magnetic moment and the Σ^0-Λ transition moment). They are being determined by a phenomenological analysis of the differential cross section data as shown in the following. The available data on the total cross section, lambda and proton polarization asymmetry, as well

as the experimental value of the branching ratio, are not being used in our fitting procedure but are compared with predictions using the models suggested by our analysis.

The experimental investigation of positive kaon photoproduction off the proton started in the late 1950s and was pursued until the early 1970s. At the present time the complete collection of the data from threshold up to 1.4 GeV contains 139 differential cross section[36–47] (see Appendix C), five total cross section,[48] 25 final-state Λ-polarization,[38,40,49–52] and three polarized target[53] measurements.

Several authors[2] have suspected the lack of consistency within the differential cross section data which have been obtained by some 12 different groups. To clear up if not the origins but at least the manifestations, the importance, and the consequences of eventual inconsistencies, we have performed a thorough study of all the available data.

We concentrate on the differential cross section, which, in contrast to asymmetry parameters, involves absolute measurements. We notice that given the number of the model's free parameters and the expected smoothness of the energy and/or angular dependence of the cross section within the phase space under consideration, the number of data points is sufficiently large. However, there are too few overlapping kinematics between different sets of experimental results to allow a direct and meaningful consistency check.

Only statistical uncertainties have been tabulated in the experimental papers and, consequently, these values have been used in all previous theoretical analyses. Nevertheless, systematic errors have been reported for more than 80% of the data points.[36–43] Given that *a priori* there is no reason to attribute higher credit to one of the data sets, no renormalization procedure can be applied using the systematic uncertainties. Being aware of these constraints, we adopted a "hybrid" method which, as explained in the following, comes out to be powerful enough for the investigation of inconsistencies within the data.

As a starting point, we limit ourselves to the experimental results for which both statistical and systematic errors ($\Delta\sigma_{\rm stat}$ and $\Delta\sigma_{\rm sys}$, respectively) have been reported (112 data points). For each point we then calculate a "total" error bar:

$$\Delta\sigma_{\rm tot}=(\Delta\sigma^2_{\rm stat}+\Delta\sigma^2_{\rm sys})^{1/2}\ .$$

Using the theoretical model as described in Sec. II B, we fit these data implementing their "total" error bars. Among the numerous possible combinations of the exchanged particles given in Table V, we look for a set by requiring reasonable values for the two main coupling constants with regard to the SU(3) predictions, small reduced chi-square per degree of freedom (χ^2/N), and reproducing well enough the Λ-polarization asymmetry measurements. We find such a set with $g_{K\Lambda N}/\sqrt{4\pi}=-3.78$, $g_{K\Sigma N}/\sqrt{4\pi}=+1.06$, and $\chi^2/N=1.2$, containing extended Born terms (Born terms $+\Sigma^0+K^*$ exchange), the $K1$ resonance, *three* nucleonic resonances ($N1$, $N3$, and $N4$), and *four* hyperonic resonances ($Y2$, $Y3$, $Y5$, and $Y6$). At the end of this subsection we will discuss the reason for the apparent need for so many resonances.

Using this model, we extract the relative deviation

$$R=\frac{d\sigma_{\rm th}-d\sigma_{\rm exp}}{\Delta\sigma_{\rm stat}}\ ,$$

with $d\sigma_{\rm th}$ ($d\sigma_{\rm exp}$) being the theoretical (experimental) differential cross section. In Fig. 2 we show the value of R for each data point (as numbered in Tables IX and X), both for data sets with known systematic errors[36–43] [Fig. 2(a)–(h)] as well as for those reported[44–47] only with statistical uncertainties [Fig. 2 (i)–(l)]. Note that our fit contains only those data sets for which systematic errors have been quoted.

The mean values of the relative deviation, $\langle R\rangle$, for all data sets are given in Table III and shown in Fig. 2 by dashed lines. This quantity corresponds to an overall model-dependent renormalization factor between different experimental sets. Notice that the mean relative

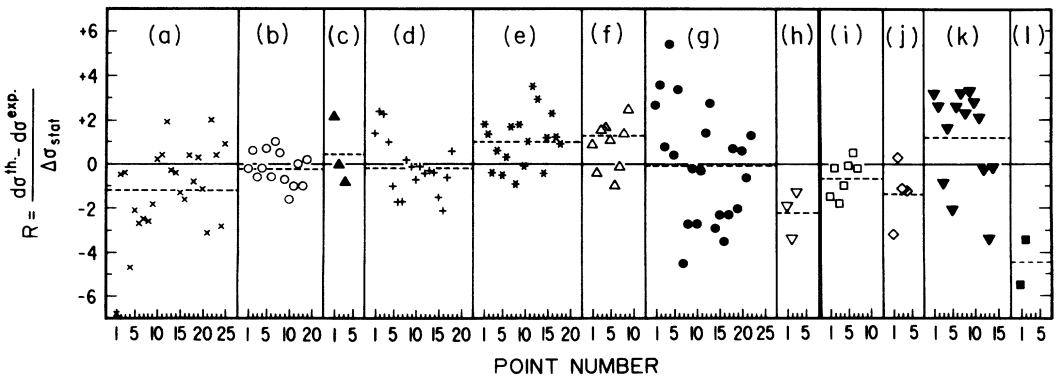

FIG. 2. Relative deviation R for each differential cross section data point for the reaction $\gamma p\to K^+\Lambda$. Points are numbered as in Tables IX and X. The data are from (a) Anderson *et al.* (Ref. 36), (b) Peck (Ref. 37), (c) Groom *et al.* (Ref. 38), (d) Bleckmann *et al.* (Ref. 39), (e) Fujii *et al.* (Ref. 40), (f) Göing *et al.* (Ref. 41), (g) Décamp *et al.* (Ref. 42), (h) Feller *et al.* (Ref. 43), (i) Donoho *et al.* (Ref. 44), (j) Brody *et al.* (Ref. 45), (k) Anderson *et al.* (Ref. 46), (l) Mori (Ref. 47). The dashed line indicates the mean value $\langle R\rangle$ for each set.

TABLE III. Mean deviation $\langle R \rangle$ for each data set shown in Fig. 2.

Data set	$\langle R \rangle$	Reference	Laboratory
(a)	−1.16	Anderson *et al.* (Ref. 36)	Cornell
(b)	−0.21	Peck (Ref. 37)	CalTech
(c)	+0.47	Groom *et al.* (Ref. 38)	CalTech
(d)	−0.15	Bleckmann *et al.* (Ref. 39)	Bonn
(e)	+1.02	Fujii *et al.* (Ref. 40)	Tokyo
(f)	+1.29	Göing *et al.* (Ref. 41)	DESY
(g)	−0.04	Décamp *et al.* (Ref. 42)	Orsay
(h)	−2.20	Feller *et al.* (Ref. 43)	Bonn
(i)	−0.61	Donoho *et al.* (Ref. 44)	CalTech
(j)	−1.30	Brody *et al.* (Ref. 45)	CalTech
(k)	+1.20	Anderson *et al.* (Ref. 46)	Cornell
(l)	−4.45	Mori (Ref. 47)	Cornell

error bars $\langle \Delta\sigma_{\text{stat}}/d\sigma_{\text{exp}} \rangle$ are roughly ±7% for all sets (a)–(h) except for that of Orsay,[42] for which it is about 2 times smaller.

At this point we can proceed to consistency checks at two levels: within each data set (*internal*) and between different data sets (*external*). If the data within a given set are coherent, then we expect them to be scattered in the vicinity of the corresponding mean deviation value $\langle R \rangle$. A close examination of the points within $\langle R \rangle \pm 2$, corresponding to the experimental values $d\sigma_{\text{exp}}$ being within $\pm 2\Delta\sigma_{\text{stat}}$ from the "mean" value, shows that such an area includes 90–100% of the points for all sets in Fig. 2, except for sets (a) and (g) for which this percentage is 83% and 45%, respectively. While the result for set (a) is quite acceptable, the one for the Orsay data [set (g)] shows a large dispersion. Even when considering $\pm 3\Delta\sigma_{\text{stat}}$ we still miss about 20% of the points. This finding reveals *internal inconsistencies within Orsay's data.* It further explains why the inclusion of these 22 incoherent data points, which cover a large domain in the phase space ($\theta_{K^+}^{\text{c.m.}} = 65° - 135°$ and $E_\gamma^{\text{lab}} = 0.97 - 1.4$ GeV), lead to unrealistic coupling constants when taken[14] only with their (small) statistical error bars. As we will discuss later, these data also bring in the disturbing need for a large number of resonances.

The *external* consistency can be clarified by comparing the mean deviations $\langle R \rangle$, hereby allowing us to establish a measure for the relative renormalization factor. The data are considered to be externally consistent if $|\langle R \rangle|$ is compatible with the statistical uncertainties, i.e., of the order 1. As shown in Table III, $\langle R \rangle$ varies from −4.5 to +1.3. Given the statistical accuracies (±7%), this corresponds to a renormalization factor of up to 40%. Disregarding sets (h) and (l), which contain too few points to be significant, this factor is reduced to about 20%.

Apart from the 22 data points in set (g) (which is internally inconsistent), and the five data points in sets (h) and (l) (which show large external inconsistencies), we infer that at the present stage of the experimental results the precision of the domain can be set at the level of 20%. Note that the "total" error bars come out to be around ±11% and, hence, using them we approach a more realistic degree of accuracy of the data. Any deeper investigation should await sufficiently accurate absolute measurements with forthcoming facilities.

This conclusion leads us to refit the data with their "total" uncertainties, excluding the data of Orsay. Notice that starting with the extended Born terms and then including *all* combinations of the resonances listed in Table V, one ends up with 4096 possibilities. While the reduced χ^2 for more than 90% of the configurations come out to be less than 1.6, the SU(3) constraints on the two main coupling constants offer a drastic selectivity: only two models fulfill these requirements. The relevant coupling constants for these two models are given in Table IV.

We remark that (i) the two main *KYN* CC's are in perfect agreement with SU(3) predictions. (ii) The couplings of the extended Born terms and $K1$ are quite stable within the two models. (iii) The reaction mechanism with

TABLE IV. Coupling constants and reduced χ^2 as obtained from our least-squares analysis. The value (Ref. 24) of μ_Λ is consistently taken to be $-0.6138\ \mu_N$, and $G_V \equiv g_{K^*K\gamma} g^V_{K^*\Lambda p}$, $G_T \equiv g_{K^*K\gamma} g^T_{K^*\Lambda p}$, $G_{N^*} \equiv g_{K\Lambda N^*} \kappa(N^*N)$, $G_{Y^*} \equiv g_{KY^*N} \kappa(Y^*\Lambda)$, $G_V^{K1} \equiv g_{K1K\gamma} g^V_{K1\Lambda p}$, $G_T^{K1} \equiv g_{K1K\gamma} g^T_{K1\Lambda p}$.

Couplings	Model 1	Model 2
$g_{K\Lambda N}/\sqrt{4\pi}$	−4.17	−4.26
$g_{K\Sigma N}/\sqrt{4\pi}$	+1.18	+1.20
$G_V/4\pi$	−0.43	−0.38
$G_T/4\pi$	+0.20	+0.30
$G_{N1}/\sqrt{4\pi}$	−1.41	−0.20
$G_{Y1}/\sqrt{4\pi}$		−2.47
$G_{Y3}/\sqrt{4\pi}$	−3.17	
$G_V^{K1}/4\pi$	−0.10	−0.06
$G_T^{K1}/4\pi$	−1.21	−1.35
χ^2/N	1.3	1.4

respect to baryonic resonances is rather simple; namely, each model contains only *one* nucleonic ($N1$) and *one* hyperonic ($Y3$ or $Y1$) resonance. (iv) The Roper resonance ($N1$) is present in both models, while its hyperonic counterpart ($Y2$) does not contribute. (v) The obtained χ^2/N values are small and comparable. From the last point we conclude that the existing differential cross section results do not allow an unambiguous determination of the reaction mechanism. We will come back to this problem in the next section where we compare the results of our models with the available differential cross section data as well as polarization measurements.

At this point it is worthwhile mentioning the sensitivity of the calculated differential cross section to the main coupling constants. A decrease (increase) of, for example, 10% in $g_{K\Lambda N}$ results[22] in a reduction (enhancement) of about 30% of the differential cross section at kaon c.m. angles larger than 45°. At smaller angles, even the slope of $d\sigma/d\Omega$ is affected. Modifying $g_{K\Sigma N}$ by the same percentage produces only a small ($\leq$ 10%) overall shift. Thus, as expected, the reaction under consideration puts stronger constraints on $g_{K\Lambda N}$ than on $g_{K\Sigma N}$. Given the accuracy of the available data, the values obtained for the two main coupling constants are reliable to better than 20%. A comprehensive error analysis on the extracted values requires data from cross section absolute measurements with realistic total uncertainties smaller than 10%.

We are now able to tackle the problems encountered by different authors (see Table I) through basically analogous phenomenological data analyses. We remind the reader that as much as the two main coupling constants are concerned, the fitting procedure provides $g_{K\Lambda N}$ and the product $\mu(\Sigma^0\Lambda)\cdot g_{K\Sigma N}$. As discussed in Appendix A, the SU(3) symmetry forces this product to be of opposite sign with regard to $g_{K\Lambda N}$. Because of interference terms in the scattering amplitude (Appendix B), the numerical values of the observables depend on this relative sign. Given $g_{\pi NN}>0$, the commonly used de Swart[5] convention sets $g_{K\Lambda N}<0$, $g_{K\Sigma N}>0$, and $\mu(\Sigma^0\Lambda)>0$. In the absence of any measurements of the Σ^0-Λ transition moment, Thom[13] and Renard and Renard[14] in their pioneer works used the SU(3) prediction $\kappa(\Sigma^0\Lambda)=+1.72$.

In 1966, the complete set of data available to Thom included 60 points. The extracted values of the main coupling constants came out to be unrealistic, leading the author to emphasize the need for more and accurate data.

By the time Renard and Renard performed their detailed investigation, all the data sets referred to in Table III were available. They included a large number of experimental results [except sets (b), (h), (i), and (j)], as well as those of Orsay[42] up to 1.70 GeV. They also fitted $p(\gamma,K^+)\Sigma^0$ data up to 1.84 GeV. As shown in Table I, the two fits give significantly different values for the main coupling constants. Particularly, those obtained from $p(\gamma,K^+)\Lambda$ are too small. In addition, their fit required 13 nucleonic and hyperonic resonances. Such a large number of resonances appeared to point to a hopelessly complicated reaction mechanism, and explains perhaps the lack of more theoretical and experimental investigations in the field for more than ten years.

The fact that Renard and Renard included data at energies higher than the one investigated in this paper does not justify the need for so many resonances. In a recent work,[54] total cross section measurements up to 2.2 GeV were reproduced with only five resonances being included. We remind the reader that our fit required seven baryonic resonances when including the Orsay data, while only two of them were necessary after excluding this set.

In the early 1980s, the projects of the new generation of electromagnetic probes suggested[55] the investigation of hypernuclei by using these facilities in the future. Following Thom's approach,[13] the study of the elementary reaction gained renewed interest, and a formalism containing only Born terms[56] was extended[3,4] to include mesonic and baryonic resonances. This operator is currently being used for the study of the elementary reaction and hypernuclei. Adelseck *et al.* used their operator to fit[3] all the data [except set (g)] and they later extended[4] the analysis to also included electroproduction data. The authors concentrated on the $K\Lambda N$ coupling constant for which they actually found (Table I) a reasonable result, while $g_{K\Sigma N}$ had too large absolute value. This situation is partly due to the fact that the included error bars (only statistical) are by now clear to overestimate the accuracy of the data.

Another source of difficulty, to our knowledge present in most recent kaon photoproduction papers, comes from the wrong sign attributed to the Σ^0-Λ transition moment of which the absolute value, $|\kappa(\Sigma^0\Lambda)|$, has been measured to be 1.82 ± 0.25 (Ref. 57), or more recently 1.59 ± 0.09 (Ref. 58). Previous authors have used either -1.82 (Refs. 2, 4, 16, and 31) or -1.59 (Ref. 54), instead of $+1.59$. The $K\Sigma N$ coupling constants quoted in Table I have been recalculated using $\kappa(\Sigma^0\Lambda)=+1.59$.

III. OBSERVABLES IN THE PROCESS $\gamma+p\rightarrow K^++\Lambda$

Contrary to the present analysis, previous investigations have often included the Λ-polarization data in the fitting procedure, thus lacking any means of testing their predictive power. Even though there exist a few data points involving a polarized proton target, other studies have not presented any results for observables other than $d\sigma/d\Omega$, P, or $\sigma_{\rm tot}$.

In this section, we examine the sensitivity of the differential and total cross section, the polarization observables, and the branching ratio to the two models established in Sec. II C. Due to the somewhat large number of polarization observables, we have made a selection illustrating their magnitudes and sensitivities to model inputs.

This section is subdivided into four subsections. We compare the differential cross section with data in the first subsection. The second subsection deals with single polarization observables, i.e., polarized target asymmetry, polarized photon asymmetry, and the polarization asymmetry of the produced lambda. Comparisons with experimental results are given as far as they are available. In the third subsection, we present our predictions for a representative sample of double polarization observables. We end this section with a brief discussion of the total

cross section and the branching ratio.

Note that in all the figures the data are shown with statistical error bars only.

A. Differential cross section, comparison with data

The following graphs demonstrate our fit of the differential cross section data. Since the data are widely scattered, we present a few selected kinematical regions which contain a reasonable number of experimental points.

The angular distribution of the differential cross section is shown in Fig. 3. We have chosen two energies to display the essential features of our model. The lower energy lies less than 90 MeV above threshold while the second one is towards the upper energy limit (1.4 GeV) of our underlying data base. The data points shown in the figure include all experimental results taken within an energy range of ± 10 MeV around the nominal value stated on the respective graph. As can be seen from Fig. 3(b), model 1 ($M1$) as well as model 2 ($M2$) (see Table IV) describe the data remarkably well. Only at extreme forward angles do we find a slight deviation.

At the lower energy, Fig. 3(a), the agreement between experiment and theory is less pronounced. Note, however, that the data have been taken from four different sets (see Sec. II C) and are scattered in such a way that it would be difficult for any smooth curve to provide a perfect fit.

Complementary to the angular distribution, we present in Fig. 4 the differential cross section as a function of energy at two different angles. Because the data at backward and extreme forward angles are rather scarce, we have chosen kaon c.m. angles of 30° and 90°. All existing data within $\pm 5°$ of the respective nominal value have been included in this figure. We find excellent agreement between theory and experiment for the excitation functions shown in Figs. 4(a) and 4(b). The only major deviation can be seen for data taken from Anderson *et al.*[46] and Feller *et al.*[43]

Summarizing the results shown in Figs. 3 and 4, we find that either of the models introduced in the preceding section provides an adequate description of the differential cross section for $E_\gamma^{\text{lab}} \leq 1.4$ GeV. The good agreement between theory and experiment gives us confidence that we have obtained a satisfactory description of the differential cross section. We discuss the remaining problem of the choice between the two models in the next subsection.

B. Single polarization observables

Because the differential cross section is not sensitive enough to the reaction mechanism, we investigate the ability of polarization observables to discriminate be-

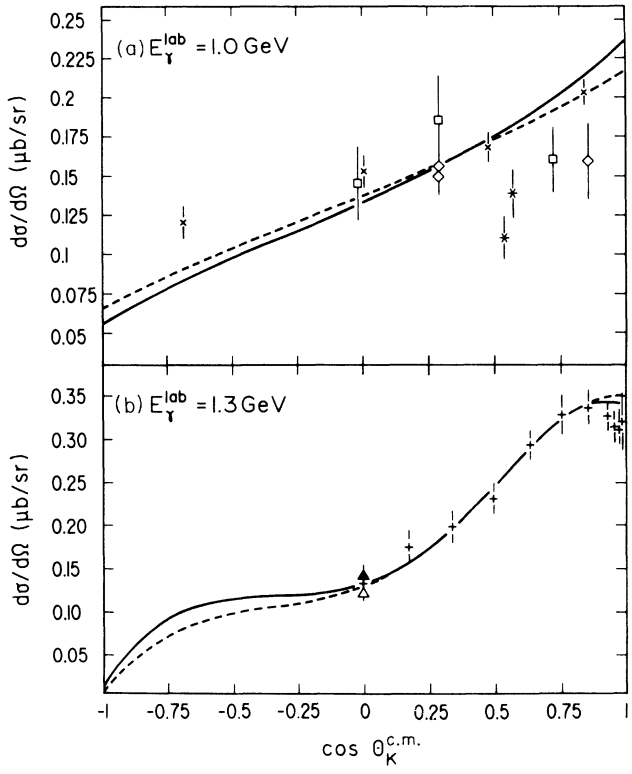

FIG. 3. Angular distribution of differential cross section for the process $\gamma p \to K^+ \Lambda$ at 1.0 GeV, (a) and 1.3 GeV, (b). The solid and dashed curves are the fits by our models 1 and 2, respectively. The symbols for the data are the same as in Fig. 2.

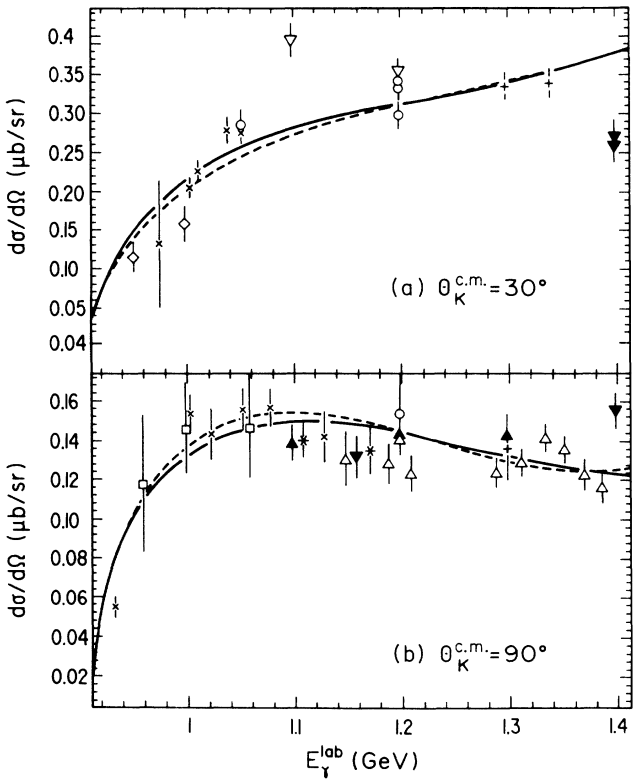

FIG. 4. Same as Fig. 3. for excitation functions at 30° and 90°.

tween the two models, $M1$ and $M2$ (Table IV).

At present, there exist no measurements of the polarized photon asymmetry Σ due to the lack of appropriate polarized photon beams. Experimental data involving a polarized target do exist,[53] but are limited to only three points with very large error bars. A more extensive data set is available for the lambda-polarization asymmetry P (Refs. 38, 40, and 49–52).

Even though the measurements are rather inaccurate, Fig. 5(a) shows that the observable P clearly prefers model 1. While $M2$ predicts only a very small polarization, even turning positive at energies higher than 1.2 GeV, the measurements provide evidence that P is rather large and negative. A similar tendency is seen in Fig. 5(b), where also the angular distribution of P has been measured to be large and negative. As in Figs. 3 and 4, we have collected all experimental results within $\pm 5°$ [Fig. 5(a)] and ± 10 MeV [Fig. 5(b)] of the nominal values. Figure 5 gives an example of how even rather imprecise measurements can lead to conclusive results.

The situation is not so obvious for the polarized target asymmetry T, shown in Fig. 6. Because of too large error bars, a decision based on the three points shown would be quite arbitrary. The present experimental results, however, are not in disagreement with our choice of $M1$ being the best model. More accurate measurements, in particular at backward kaon c.m. angles, are desirable.

The asymmetry parameter T as predicted by $M1$ at small kaon angles is almost indistinguishable from the prediction by $M2$. At large angles, however, the predictions differ by more than a factor of 5. With increasing photon lab energy the absolute difference between the predictions based on $M1$ and $M2$ increases rapidly as the kaon angle goes beyond 90°. Thus, for the observable T, measurements at backward kaon angles and above a photon energy of 1.1 GeV are strongly suggested.

For completeness we show the energy dependence of the polarized photon asymmetry parameter Σ in Fig. 7. This observable is not as sensitive as the parameter T, but it still can allow for a discrimination between the two models. For this purpose, measurements at a kaon c.m. angle around 90° and at photon lab energies above 1.1 GeV are to be preferred. At backward angles the selectivity with respect to the underlying mechanism is still

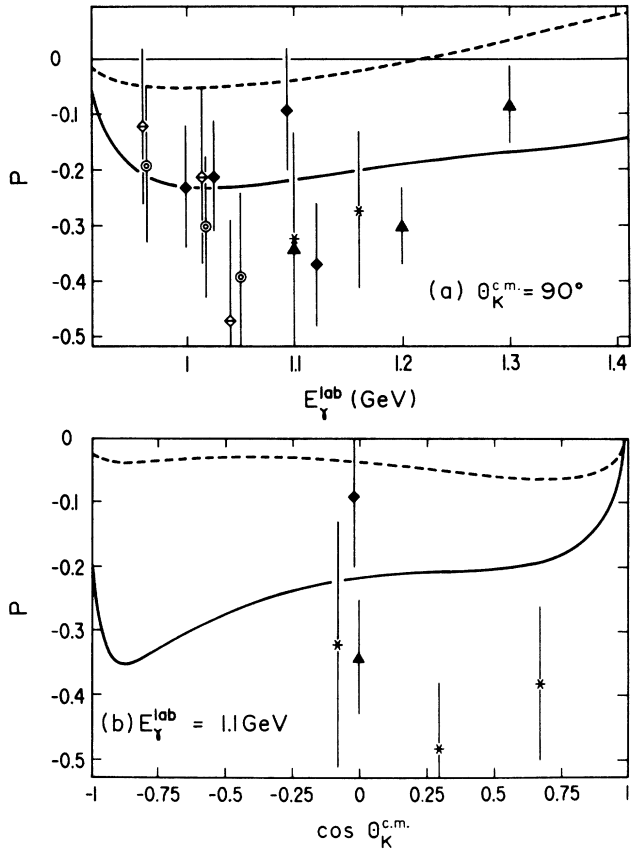

FIG. 5. Λ-polarization asymmetry in $\gamma p \to K^+ \vec{\Lambda}$ (a) as a function of photon energy at a kaon c.m. angle of 90°, and (b) as a function of kaon angle at 1.1 GeV. The data are from Thom *et al.* (Ref. 49) (♦), Borgia *et al.* (Ref. 50) (◈), Grilli *et al.* (Ref. 51) (◎), Groom *et al.* (Ref. 38) (▲), and Fujii *et al.* (Ref. 40) (*). The curves are the prediction of our models as referred to in Fig. 3.

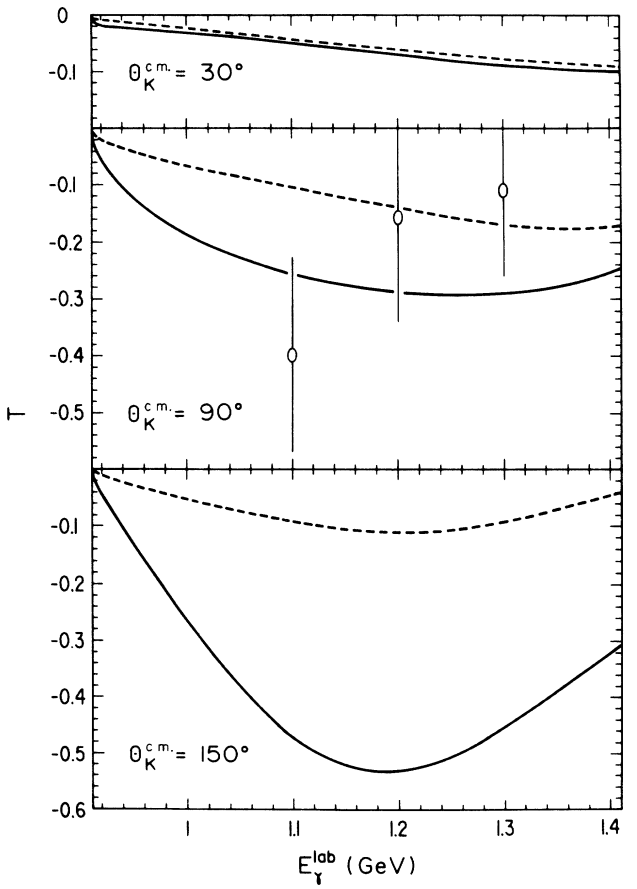

FIG. 6. Polarized target asymmetry in $\gamma \vec{p} \to K^+ \Lambda$ at three kaon angles as a function of incident beam energy. Data are at 90° and are from Althoff *et al.* (Ref. 53); curves are the same as in Fig. 3.

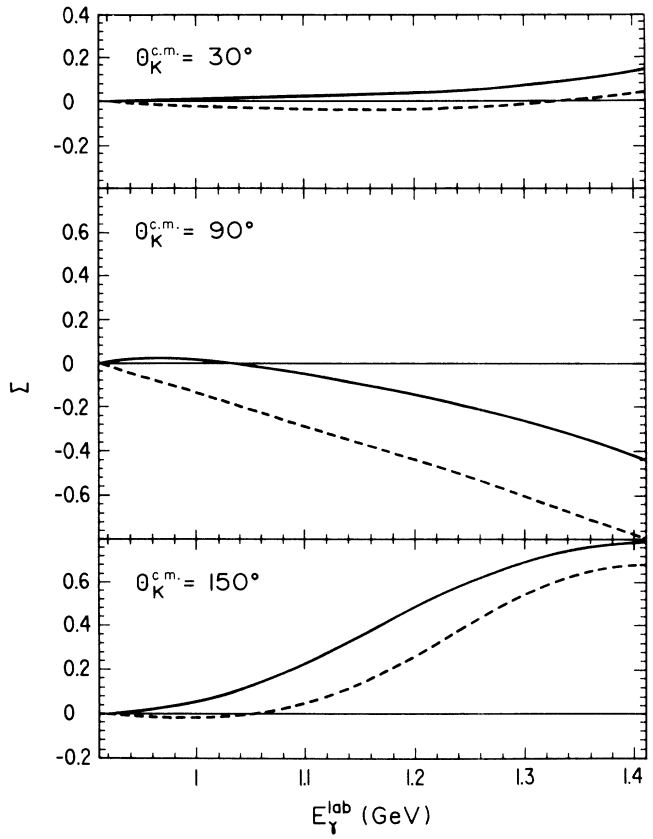

FIG. 7. Same as Fig. 6. for polarized beam asymmetry Σ in $\vec{\gamma}p \to K^+\Lambda$.

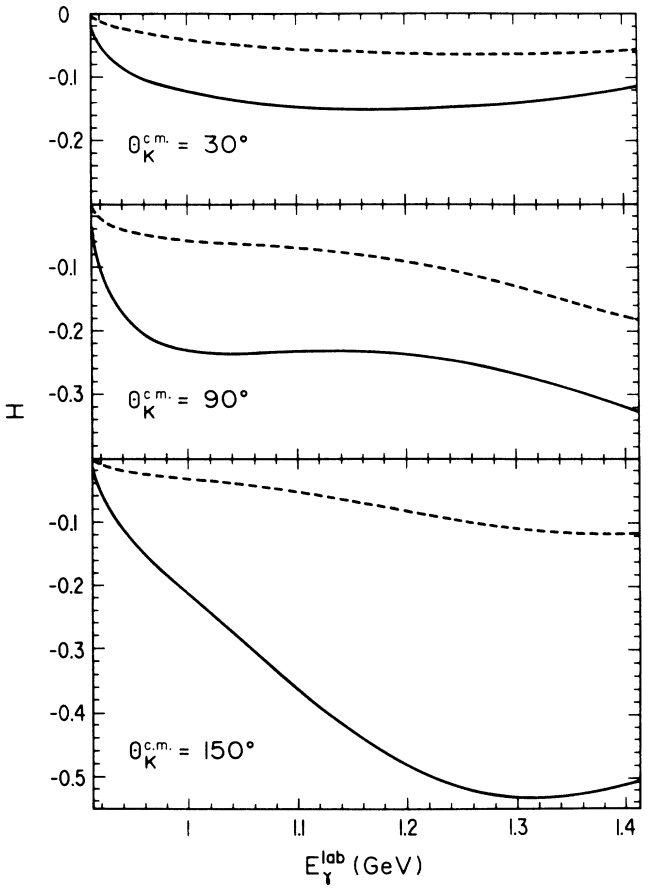

FIG. 9. Energy dependence of the observable H in $\vec{\gamma}\vec{p} \to K^+\Lambda$ at three kaon angles; curves are the same as in Fig. 3.

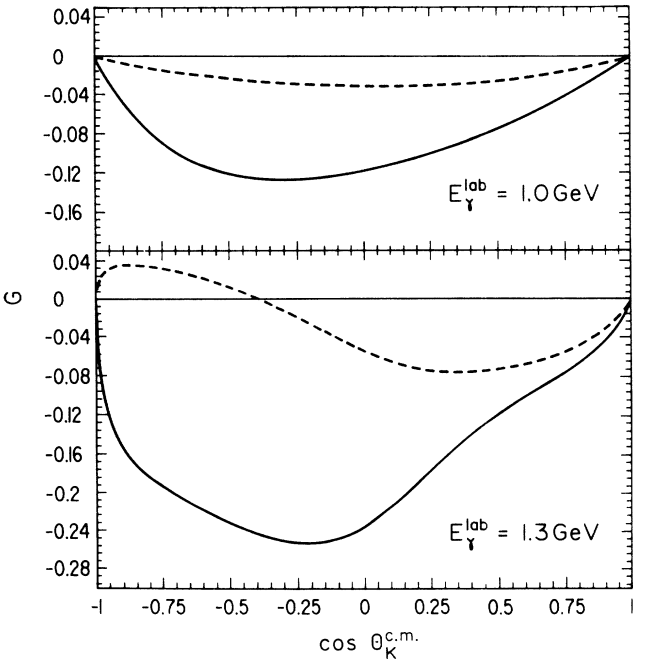

FIG. 8. Angular distribution of the observable G in $\vec{\gamma}\vec{p} \to K^+\Lambda$ at (a) 1.0 GeV and (b) 1.3 GeV; curves are the same as in Fig. 3.

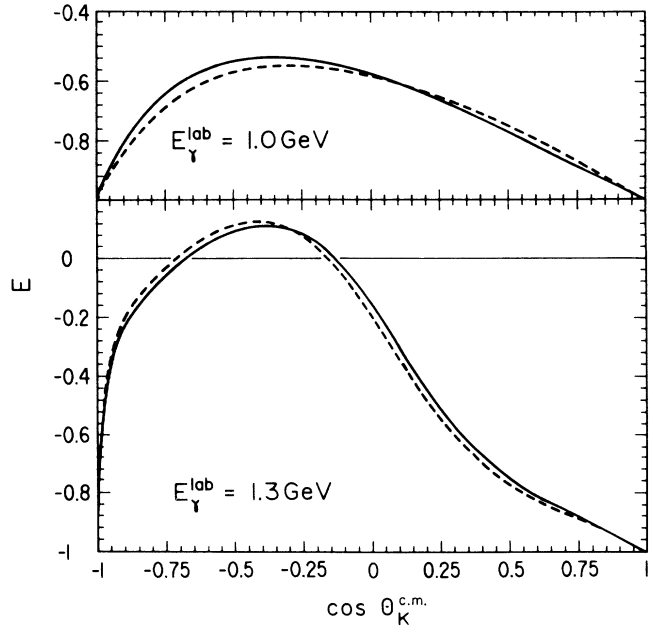

FIG. 10. Same as Fig. 9 for the observable E in the reaction $\vec{\gamma}\vec{p} \to K^+\Lambda$.

appreciable, while diminishing drastically at forward angles.

C. Double polarization observables

Having in mind the polarized beam facilities under construction, we present predictions for the observables involving a polarized photon beam, and requiring either a polarized proton target (E, G, and H), or the measurement of the lambda-polarization asymmetry (O_x).

To demonstrate the usefulness of these observables in revealing the underlying reaction mechanism, models 1 and 2 from Sec. III A are taken as representative examples for conceivable mechanisms being indistinguishable by measurements of the differential cross section alone. Although we have already concluded that $M1$ is the proper candidate (Sec. III B), we still use both modes to exemplify the sensitivity of double polarization observables.

First, we discuss the set of asymmetry observables measurable by polarized beam and target, i.e., by investigating the process $\vec{\gamma}\vec{p}\rightarrow K^+\Lambda$: E,F,G,H. Using a linearly polarized photon beam ($\pm\pi/4$ with respect to scattering plane) and a proton with its spin aligned along the photon beam axis allows the measurement of the observable G. The angular distribution of G, presented in Fig. 8, proves that this observable may serve as a good analyzer of the kaon photoproduction mechanism due to the different magnitudes and shapes of the curves predicted by the two models. A suitable choice of the kinematics for this observable lies at photon energies above 1.2 GeV and kaon c.m. angles larger than 90°.

A similar observable, the parameter H, is shown in Fig. 9. It requires the same polarization of the beam as G but with the proton spin aligned along the x axis as defined in Table II. In contrast to G, the two predicted curves do not show any structure. The most appropriate kinematics is found at about the same energy range and kaon angle as for the observable G. A quite different behavior is seen for the observable E. A measurement of the asymmetry parameter E requires the same target polarization as the observable G but with a circularly polarized photon beam. The excitation function of E is displayed in Fig. 10. The observable E, like the differential cross section $d\sigma/d\Omega$, shows only little sensitivity to the basic mechanism.

The only other observable, F, in the set of beam-target asymmetry parameters demonstrates differences between the two models of up to 30%. The kinematical region where such effects occur is at large angles ($>$ 125°) and at energies higher than 1.2 GeV.

Measuring the polarization asymmetry of the produced lambda using either a linearly or a circularly polarized beam ($\vec{\gamma}p\rightarrow K^+\vec{\Lambda}$) results in four more observables: C_x, C_z, O_x, O_z. As an example, we give in Fig. 11 the angular distribution of the observable O_x. The parameter O_x is a measure of the lambda-polarization asymmetry along an axis parallel to the x' direction (Table II) produced by a linearly polarized photon beam ($\pm\pi/4$ with respect to scattering plane). Large effects show up only at extreme backward angles and high photon energies

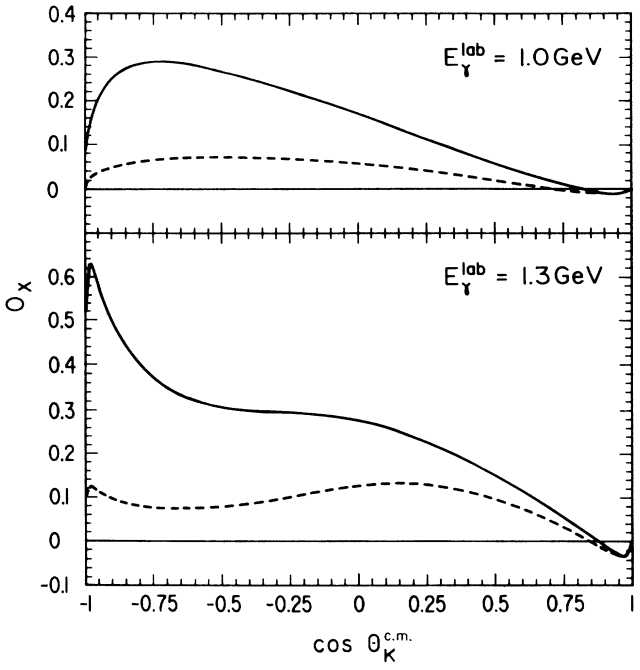

FIG. 11. Same as Fig. 8 for the observable O_x in $\vec{\gamma}p\rightarrow K^+\vec{\Lambda}$.

where $M1$ predicts a large positive peak in the asymmetry, while $M2$ remains basically flat and rather small over the full angular range.

As far as the remaining observables in this set are concerned, we find that C_z, just like E, is not particularly sensitive to the reaction mechanism. The observable C_x displays relative differences of about 20% between 1.2 and 1.3 GeV photon energy and at kaon angles between 120° and 140°. The predicted asymmetry in its region is very large, making this observable an interesting object to be studied. At energies higher than 1 GeV and angles larger than 80° we find the predictions of the asymmetry parameter O_z to differ by as much as a factor of 2. The

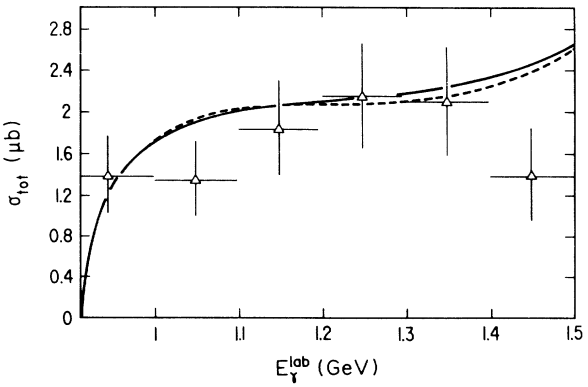

FIG. 12. Total cross section for the reaction $\gamma p\rightarrow K^+\Lambda$ as a function of photon energy. Data com from Ref. 48; curves are the same as in Fig. 3.

magnitude of the asymmetry is, however, rather small ($\sim 0.2-0.3$).

The last four observables T_x, T_z, L_x, L_z concern measurements in the reaction $\gamma \vec{p} \rightarrow K^+ \vec{\Lambda}$. We find that none of these observables provides an efficient tool for the study of the fundamental reaction mechanism. Although the asymmetries are in general quite large, there is not much difference between the predictions of models 1 and 2.

D. Total cross section and branching ratio

We end this section with a brief presentation of the total cross section and the branching ratio.

In Fig. 12, a comparison between the total cross section data and our theoretical predictions is shown. We find very good agreement between experiment and theory up to 1.4 GeV. This agreement is not surprising, since we know from Sec. III A that our models provide a reliable description of the differential cross section. At higher photon energies our predictions of the total cross section, as well as of the differential cross section, tend to grossly overestimate the experimental results. A possible explanation for this might be the hadronic character of the photon which suppresses the photoproduction channel at higher energies. A different explanation involving higher mass/spin resonant states and including absorptive effects have been given by Tanabe *et al.*[54]

Considering radiative kaon capture at rest, we obtain knowledge on the dynamics restricted to only one point in phase space. Nevertheless, this process can provide useful information since it probes a region of the amplitude which is not accessible via the photoproduction process.

The branching ratio, defined by $\Gamma(K^- p \rightarrow \Lambda\gamma)/\Gamma(K^- p \rightarrow \text{all})$, was measured in 1982 at CERN (Ref. 59) to be $(2.8\pm0.8)\times10^{-3}$. A very recent and more reliable experiment at Brookhaven[60] sets this value at $(0.86\pm0.12)\times10^{-3}$. Taking only the contributions from the Born terms, including K^* and Σ^0 exchange, we obtain for model 1 and model 2 the values 3.9×10^{-3} and 4.3×10^{-3}, respectively, which are in gross disagreement with the best measured value. Because of a large number of open questions in the field, any further discussion about this subject lies beyond the scope of this paper. For a review of the experimental and theoretical problems we refer the reader to a recent review article by Lowe.[61]

IV. SUMMARY AND CONCLUSIONS

In this paper, we have presented a comprehensive study of observables in the process of kaon photoproduction off free protons, $\gamma + p \rightarrow K^+ + \Lambda$. A model for the scattering amplitude was developed employing a diagrammatic technique. Due to the Lorentz-invariant structure of this formalism, the so constructed operator can easily be transformed into any reference frame and, thus, can readily be incorporated into hypernuclear calculations.

Using our model, we have performed a thorough analysis of all the existing differential cross sections incorporating the systematic uncertainties. This study reveals, on one hand, internal inconsistencies in the Orsay data of Décamp *et al.*[42] and, on the other hand, allows us to establish an external consistency at the level of 20% between almost all the other data sets.

Our findings enable us to clear up the reasons for the difficulties encountered in previous phenomenological investigations. Excluding the data of the Orsay group,[42] which bring in unnecessary resonances in order to account for spurious structure introduced into the differential cross section, we obtain a rather simple reaction mechanism. We further find that the extracted main coupling constants for the $K\Lambda N$ and $K\Sigma N$ vertices come out in agreement with SU(3) predictions.

Having obtained two models which adequately reproduce the differential and total cross sections, we investigate the ability of other observables to provide additional constraints on the reaction mechanism. The existing data on Λ-polarization asymmetry and, to a lesser extent, the fewer polarized target measurements, show, in spite of their poor accuracies, a clear preference for one of the two models. Besides the Born terms, our best model contains the exchange of the following particles: $K^*(892)$, $K1(1280)$, Σ^0, $N^*(1440)$, and $\Lambda^*(1670)$.

Applying crossing symmetry we relate the photoproduction amplitude to the amplitude describing the radiative capture of kaons $p(K^-,\gamma)\Lambda$. We find the prediction of our model to overestimate the latest measured value[60] of the branching ratio $\Gamma(K^- p \rightarrow \gamma\Lambda)/\Gamma(K^- p \rightarrow \text{all})$ by a factor of about 5.

We believe that the operator presented here and the set of extracted coupling constants provide a fairly accurate description of the elementary process $\gamma p \rightarrow K^+ \Lambda$ up to a photon lab energy of 1.4 GeV. At higher energies, our predictions are too large compared to the measured differential cross sections. Studies in this energy regime should probably invoke the vector meson dominance model and/or include higher mass/spin resonances. Possible manifestations of other mechanisms like off-shell effects or quark content of the hadrons might also need investigation.

A complete and unique determination of the scattering amplitude requires extended knowledge of nine observables. Nevertheless, measurements on seven of them suffice to determine the amplitudes up to phase factors.

Taking into account the state of the art, we put forward suggestions for future measurements. These can be divided into three categories according to the needed accuracies and the experimental requirements.

Absolute measurements of the differential cross section over a wide range of the phase space with total error bars smaller than $\pm10\%$ will put strong enough constraints on the extracted coupling constants. This will also allow us to settle the gross features of the reaction mechanism.

Further refinements on the latter aspect require knowledge of polarization asymmetries involving only *relative* measurements. Single polarization data at backward kaon angles with accuracies of about $\pm20\%$ would be of great help. The most favorable energy ranges for the observables T and P are expected to be at ~ 1.2 GeV

and ≥ 1.0 GeV, respectively, while for the polarized beam asymmetry Σ the sensitivity increases with the energy.

For double polarization observables the most favorable experiments require a linearly polarized photon beam, and are found in the reactions $\vec{\gamma}\vec{p}\rightarrow K^+\Lambda$ and $\vec{\gamma}p\rightarrow K^+\vec{\Lambda}$. The observables G, H, and O_x measured in kaon backward kinematics around 1.2 GeV and with an accuracy of only $\pm 30\%$ offer additional means to deepen our understanding of the underlying mechanisms.

We have shown the benefits to be gained by measuring the differential cross section, single- and/or double-polarization observables. Such extensive experimental investigations are expected to be realized in the near future by taking advantage of the accelerators at Bates, Bonn, Continuous Electron Beam Accelerator Facility (CEBAF), and European Synchrotron Radiation Facility (ESRF).

We are grateful to P. Y. Bertin for stimulating discussions.

APPENDIX A

With respect to the main kaon-hyperon-nucleon coupling constants, our formalism for the kaon-photoproduction process provides $g_{K\Lambda N}$ and the product $\mu(\Sigma^0\Lambda)\cdot g_{K\Sigma N}$. As summarized in the following, the SU(3) symmetry puts constraints on these quantities.[5,62]

(a) KYN coupling constants. The unbroken SU(3) symmetry, using de Swart's convention,[5] predicts

$$g_{K\Lambda N}=-(1/\sqrt{3})(3-2\alpha_D)g_{\pi NN} \tag{A1}$$

and

$$g_{K\Sigma N}=+(2\alpha_D-1)g_{\pi NN}\ , \tag{A2}$$

with $\alpha_D=D/(D+F)$ the fraction of D-type coupling. Taking $g^2_{\pi NN}/4\pi=14.3\pm 0.2$ (Ref. 63) and $\alpha_D=0.644\pm 0.006$ (Ref. 64), the two main KYN couplings are determined with accuracies better than 5%. But given that the SU(3) symmetry is broken at the level of 20% (Ref. 65) and by using (A1) and (A2), one obtains the following ranges for the coupling constants:

$$g_{K\Lambda N}/\sqrt{4\pi}=-4.4 \text{ to } -3.0\ ,$$

$$g_{K\Sigma N}/\sqrt{4\pi}=+0.9 \text{ to } +1.3\ .$$

(b) Σ^0-Λ transition moment. Following the convention by de Swart,[5] the Σ^0-Λ transition moment is given by

$$\mu(\Sigma^0\Lambda)=-\tfrac{1}{2}\sqrt{3}\mu(n)=+1.65\ \mu_N\ ,$$

with $\mu(n)$ the neutron magnetic moment.[24] Only the absolute value of the transition moment can be measured, and the two available experimental results[57,58] are in agreement with the SU(3) predictions.

Another convention, discussed in detail by Gibson and Pollard[62] reverses the signs of both $\mu(\Sigma^0\Lambda)$ and $g_{K\Sigma N}$ but leaves the $K\Lambda N$ vertex unchanged. Hence, the choice of the convention determines not only the sign of the transition moment, but also the signs at the strong vertices.[66] As expected, both conventions lead to the same result for the only physically meaningful sign, that between $g_{K\Lambda N}$ and $g_{K\Sigma N}\cdot\mu(\Sigma^0\Lambda)$.

In the literature, while for the strong coupling constants de Swart's convention is currently used, the sign of the transition moment (e.g., Refs. 24 and 58) is often implicitly inferred from Gibson-Pollard convention. This confusion results in a wrong relative sign between $g_{K\Lambda N}$ and $g_{K\Sigma N}\cdot\mu(\Sigma^0\Lambda)$. In this paper we consistently use de Swart's convention.

APPENDIX B

Table V lists all states considered in the present study. Tables VI–VIII, however, show only those ingredients which are relevant for our best model, i.e., the rather complicated vertex factors, propagators, and amplitudes involving nucleonic spin-$\frac{3}{2}$ resonances have been omitted.

TABLE V. Particles (Ref. 24) considered in this study; values for mass and width as used in our calculation are given in parentheses in the first and last columns, respectively.

Particle	J^π	Mass (MeV)	Width (MeV)
p	$\frac{1}{2}^+$	938.2796	
K^+	0^-	493.667	
Λ	$\frac{1}{2}^+$	1115.6	
Σ^0	$\frac{1}{2}^+$	1192.46	
K^{*+}	1^-	892.1	51.3
$K1(1280)$	1^+	1260–1280	70–110(90)
$N1(1440)$	$\frac{1}{2}^+$	1400–1480	120–350(200)
$N2(1520)$	$\frac{3}{2}^-$	1510–1530	100–140(125)
$N3(1535)$	$\frac{1}{2}^-$	1520–1560	100–250(150)
$N4(1650)$	$\frac{1}{2}^-$	1620–1680	100–200(150)
$N5(1700)$	$\frac{3}{2}^-$	1670–1730	70–120(100)
$N6(1710)$	$\frac{1}{2}^+$	1680–1740	90–130(110)
$N7(1720)$	$\frac{3}{2}^+$	1690–1800	125–250(200)
$Y1(1405)$	$\frac{1}{2}^-$	1405	30–50(40)
$Y2(1600)$	$\frac{1}{2}^+$	1560–1700	50–250(150)
$Y3(1670)$	$\frac{1}{2}^-$	1660–1680	25–50(35)
$Y4(1800)$	$\frac{1}{2}^-$	1720–1850	200–400(300)
$Y5(1800)$	$\frac{1}{2}^+$	1750–1850	50–250(150)
$Y6(1660)$	$\frac{1}{2}^+$	1630–1690	40–200(100)
$Y7(1750)$	$\frac{1}{2}^-$	1730–1820	60–160(90)

TABLE VI. Vertex factors corresponding to the Feynman diagrams (Fig. 2). $M=1$ GeV is inserted to render $g_{K^*K\gamma}$ and $g_{K1K\gamma}$ dimensionless. The magnetic moments μ are related to κ by $\mu=\kappa e\hbar/2M_p$.

Vertex	Coupling
$pp\gamma$	$e\gamma\cdot\varepsilon+\mu_p\gamma\cdot p_\gamma\gamma\cdot\varepsilon$
$K^+\Lambda p$	$ig_{K\Lambda p}\gamma_5$
$K^+K^+\gamma$	$e\varepsilon\cdot(2p_K-p_\gamma)$
$\Lambda\Lambda\gamma$	$\mu_\Lambda\gamma\cdot p_\gamma\gamma\cdot\varepsilon$
$\Sigma\Lambda\gamma$	$\mu(\Sigma^0\Lambda)\gamma\cdot p_\gamma\gamma\cdot\varepsilon$
$K^+\Sigma p$	$ig_{K\Sigma p}\gamma_5$
$K^*K^+\gamma$	$\frac{g_{K^*K\gamma}}{M}\varepsilon^{\mu\nu\rho\sigma}\varepsilon_\nu(p_\gamma)_\rho(p_\Lambda-p_p)_\sigma$
$K^*\Lambda p$	$g^V_{K^*\Lambda p}\gamma^\mu+\frac{g^T_{K^*\Lambda p}}{M_\Lambda+M_p}(\gamma\cdot p_\Lambda-\gamma\cdot p_p)\gamma^\mu$
$K1K^+\gamma$	$\frac{g_{K1K\gamma}}{M}(p_\gamma\cdot(p_K-p_\gamma)\varepsilon^\mu-\varepsilon\cdot(p_K-p_\gamma)p_\gamma^\mu)$
$K1\Lambda p$	$g^V_{K1\Lambda p}\gamma^\mu\gamma_5+\frac{g^T_{K1\Lambda p}}{M_\Lambda+M_p}(\gamma\cdot p_\Lambda-\gamma\cdot p_p)\gamma^\mu\gamma_5$
$N^*(\frac{1}{2})^+p\gamma$	$\mu(N^*N)\gamma\cdot p_\gamma\gamma\cdot\varepsilon$
$K^+\Lambda N^*(\frac{1}{2})^+$	$ig_{K\Lambda N^*}\gamma_5$
$Y^*(\frac{1}{2})^+\Lambda\gamma$	$\mu(Y^*\Lambda)\gamma\cdot p_\gamma\gamma\cdot\varepsilon$
$K^+Y^*(\frac{1}{2})^+p$	$ig_{KY^*N}\gamma_5$

TABLE VII. Propagators for particles of mass M, width Γ, four-momentum q, and spin 0, $\frac{1}{2}$, and 1.

Spin	Propagator
0	$\frac{1}{q^2-M^2+iM\Gamma}$
$\frac{1}{2}$	$\frac{\gamma\cdot q+M}{q^2-M^2+iM\Gamma}$
1	$\frac{1}{q^2-M^2+iM\Gamma}\left[-g_{\mu\nu}+\frac{q_\mu q_\nu}{M^2}\right]$

TABLE VIII. Contributions to the invariant scattering amplitude arising from the exchange of (a) the Born terms (including K^{*+} and Σ exchange), (b) the $K1$, (c) the nucleonic $J^\pi=\frac{1}{2}^\pm$ states, (d) the hyperonic $J^\pi=\frac{1}{2}^\pm$ states. $g_\Lambda\equiv g_{K\Lambda p}$, $g_\Sigma\equiv g_{K\Sigma p}$, $G_V\equiv g_{K^*K\gamma}g^V_{K^*\Lambda p}$, $G_T\equiv g_{K^*K\gamma}g^T_{K^*\Lambda p}$, $G^{K1}_V\equiv ig_{K1K\gamma}g^V_{K1\Lambda p}$, $G^{K1}_T\equiv g_{K1K\gamma}g^T_{K1\Lambda p}$, $G_{N^*}\equiv g_{K\Lambda N^*}\kappa(N^*N)$, $G_{Y^*}\equiv g_{KY^*N}\kappa(Y^*\Lambda)$.

Born terms

$$\mathcal{A}_1^{\text{Born}}=\frac{g_\Lambda e}{s-M_p^2}(1+\kappa_p)+\frac{g_\Lambda e}{u-M_\Lambda^2}\frac{M_\Lambda\kappa_\Lambda}{M_p}+\frac{g_\Sigma e}{u-M_\Sigma^2}\frac{(M_\Sigma+M_\Lambda)\kappa(\Sigma^0\Lambda)}{2M_P}$$
$$+\frac{G_V}{M}\frac{M_\Lambda+M_p}{t-M_{K^*}^2+iM_{K^*}\Gamma_{K^*}}+\frac{G_T}{M}\frac{t}{M_\Lambda+M_p}\frac{1}{t-M_{K^*}^2+iM_{K^*}\Gamma_{K^*}}$$

$$\mathcal{A}_2^{\text{Born}}=\frac{2g_\Lambda e}{(s-M_p^2)(t-M_K^2)}+\frac{G_T}{M}\frac{1}{M_\Lambda+M_p}\frac{1}{t-M_{K^*}^2+iM_{K^*}\Gamma_{K^*}}$$

$$\mathcal{A}_3^{\text{Born}}=\frac{g_\Lambda e}{s-M_p^2}\frac{\kappa_p}{M_p}+\frac{G_V}{M}\frac{1}{t-M_{K^*}^2}-\frac{G_T}{M}\frac{M_\Lambda-M_p}{M_\Lambda+M_p}\frac{1}{t-M_{K^*}^2+iM_{K^*}\Gamma_{K^*}}$$

$$\mathcal{A}_4^{\text{Born}}=\frac{g_\Lambda e}{u-M_\Lambda^2}\frac{\kappa_\Lambda}{M_p}+\frac{g_\Sigma e}{u-M_\Sigma^2}\frac{\kappa(\Sigma^0\Lambda)}{M_p}+\frac{G_V}{M}\frac{1}{t-M_{K^*}^2+iM_{K^*}\Gamma_{K^*}}+\frac{G_T}{M}\frac{M_\Lambda-M_p}{M_\Lambda+M_p}\frac{1}{t-M_{K^*}^2+iM_{K^*}\Gamma_{K^*}}$$

TABLE VIII. (*Continued*).

$K1$

$$\mathcal{A}_1^{K1}=0$$

$$\mathcal{A}_2^{K1}=-\frac{G_T^{K1}}{M}\frac{1}{M_\Lambda+M_p}\frac{1}{t-M_{K1}^2+\epsilon' M_{K1}\Gamma_{K1}}$$

$$\mathcal{A}_3^{K1}=\frac{G_V^{K1}}{M}\frac{1}{t-M_{K1}^2+\epsilon' M_{K1}\Gamma_{K1}}+\frac{G_T^{K1}}{M}\frac{M_\Lambda-M_p}{M_\Lambda+M_p}\frac{1}{t-M_{K1}^2+\epsilon' M_{K1}\Gamma_{K1}}$$

$$\mathcal{A}_4^{K1}=-\frac{G_V^{K1}}{M}\frac{1}{t-M_{K1}^2+\epsilon' M_{K1}\Gamma_{K1}}-\frac{G_T^{K1}}{M}\frac{M_\Lambda-M_p}{M_\Lambda+M_p}\frac{1}{t-M_{K1}^2+\epsilon' M_{K1}\Gamma_{K1}}$$

Nucleonic $J^\pi=\frac{1}{2}^\pm$

$$\mathcal{A}_1^{N^*(1/2)^\pm}=\frac{g_{K\Lambda N^*}e}{s-M_{N^*}^2+\epsilon' M_{N^*}\Gamma_{N^*}}\frac{(M_{N^*}+M_p)\kappa(N^*N)}{2M_p}\frac{M_{N^*}-M_p}{M_{N^*}\mp M_p}$$

$$\mathcal{A}_2^{N^*(1/2)^\pm}=0$$

$$\mathcal{A}_3^{N^*(1/2)^\pm}=\pm\frac{g_{K\Lambda N^*}e}{s-M_{N^*}^2+\epsilon' M_{N^*}\Gamma_{N^*}}\frac{\kappa(N^*N)}{M_p}$$

$$\mathcal{A}_4^{N^*(1/2)^\pm}=0$$

Hyperonic $J^\pi=\frac{1}{2}^\pm$

$$\mathcal{A}_1^{Y^*(1/2)^\pm}=\frac{g_{KY^*N}e}{u-M_{Y^*}^2+\epsilon' M_{Y^*}\Gamma_{Y^*}}\frac{(M_{Y^*}+M_\Lambda)\kappa(Y^*\Lambda)}{2M_p}\frac{M_{Y^*}-M_\Lambda}{M_{Y^*}\mp M_\Lambda}$$

$$\mathcal{A}_2^{Y^*(1/2)^\pm}=0$$

$$\mathcal{A}_3^{Y^*(1/2)^\pm}=0$$

$$\mathcal{A}_4^{Y^*(1/2)^\pm}=\pm\frac{g_{KY^*N}e}{u-M_{Y^*}^2+\epsilon' M_{Y^*}\Gamma_{Y^*}}\frac{\kappa(Y^*\Lambda)}{M_p}$$

APPENDIX C

We give the complete data base of the existing differential cross section data. A large number of these results, with a few misprints, can be found in the compilation by Genzel *et al.*[67]

Table IX shows all the data sets with known systematic errors and for which we have calculated "total" uncertainties (see Sec. II C). The data sets reported with only statistical errors are presented in Table X.

TABLE IX. Differential cross section data for the reaction $p(\gamma,K^+)\Lambda$ with statistical errors, and "total" uncertainties given in parentheses (see Sec. II C). The first column numbers the data points as referred to in Fig. 2.

No.	E_γ^{lab} (GeV)	$\theta_K^{c.m.}$ (deg)	$d\sigma/d\Omega^{c.m.}$ (μb/sr)	Reference
1	0.934	90.0	0.055±0.004(0.007)	
2	0.974	64.0	0.133±0.080(0.081)	
3	0.976	31.1	0.134±0.080(0.081)	
4	1.002	30.0	0.204±0.007(0.022)	
5	1.003	60.3	0.169±0.009(0.019)	
6	1.004	88.6	0.154±0.009(0.018)	
7	1.004	132.0	0.121±0.010(0.016)	
8	1.013	30.3	0.228±0.011(0.025)	
9	1.018	55.6	0.200±0.010(0.022)	
10	1.018	97.0	0.133±0.006(0.015)	
11	1.020	43.6	0.196±0.011(0.022)	
12	1.022	69.8	0.155±0.008(0.017)	
13	1.024	94.2	0.145±0.011(0.018)	Anderson *et al.*
14	1.036	45.0	0.230±0.008(0.024)	(Ref. 36)
15	1.040	27.5	0.281±0.014(0.031)	
16	1.051	80.2	0.196±0.012(0.023)	
17	1.054	30.0	0.276±0.015(0.031)	
18	1.054	53.5	0.244±0.014(0.028)	
19	1.054	89.7	0.157±0.009(0.018)	
20	1.055	42.5	0.271±0.013(0.030)	
21	1.060	132.3	0.123±0.011(0.017)	
22	1.080	46.5	0.244±0.012(0.027)	
23	1.080	90.0	0.158±0.008(0.018)	
24	1.080	119.7	0.125±0.008(0.015)	
25	1.130	90.0	0.142±0.013(0.019)	
1	1.054	31.0	0.284±0.022(0.028)	
2	1.054	48.0	0.233±0.019(0.024)	
3	1.080	46.5	0.279±0.018(0.025)	
4	1.200	15.0	0.379±0.027(0.035)	
5	1.200	25.0	0.334±0.015(0.025)	
6	1.200	30.0	0.341±0.019(0.028)	
7	1.200	35.0	0.300±0.014(0.023)	Peck (Ref. 37)
8	1.200	42.0	0.284±0.015(0.023)	
9	1.200	49.0	0.282±0.016(0.023)	
10	1.200	55.0	0.276±0.016(0.023)	
11	1.200	63.0	0.241±0.016(0.022)	
12	1.200	70.0	0.202±0.014(0.019)	
13	1.200	78.0	0.194±0.017(0.021)	
14	1.200	85.0	0.154±0.018(0.020)	
1	1.100	89.9	0.139±0.009(0.017)	
2	1.200	90.2	0.143±0.007(0.016)	Groom *et al.*
3	1.300	89.8	0.143±0.009(0.019)	(Ref. 38)
1	1.300	6.0	0.321±0.033(0.037)	
2	1.300	10.0	0.314±0.020(0.025)	
3	1.300	15.0	0.316±0.016(0.022)	
4	1.300	20.0	0.328±0.013(0.021)	
5	1.300	30.0	0.337±0.018(0.025)	
6	1.300	40.0	0.330±0.020(0.026)	
7	1.300	50.0	0.295±0.015(0.021)	
8	1.300	60.0	0.233±0.015(0.019)	
9	1.300	70.0	0.200±0.017(0.020)	Bleckmann *et al.*
10	1.300	80.0	0.176±0.018(0.020)	(Ref. 39)
11	1.300	90.0	0.137±0.017(0.018)	
12	1.327	62.0	0.239±0.020(0.023)	
13	1.332	52.7	0.270±0.022(0.026)	
14	1.336	43.2	0.299±0.020(0.025)	
15	1.340	33.5	0.340±0.019(0.025)	
16	1.342	23.3	0.361±0.015(0.023)	
17	1.343	17.7	0.349±0.018(0.025)	
18	1.344	11.2	0.334±0.025(0.030)	
1	0.994	56.6	0.112±0.012(0.016)	
2	1.005	54.0	0.141±0.013(0.018)	
3	1.047	50.5	0.237±0.015(0.026)	
4	1.047	78.0	0.172±0.011(0.019)	
5	1.064	49.0	0.259±0.017(0.029)	
6	1.064	76.0	0.187±0.009(0.019)	
7	1.090	48.0	0.248±0.012(0.025)	
8	1.090	73.5	0.209±0.010(0.021)	
9	1.090	96.0	0.132±0.008(0.014)	Fujii *et al.*
10	1.110	72.5	0.204±0.013(0.022)	(Ref. 40)
11	1.110	93.5	0.141±0.008(0.015)	
12	1.113	47.5	0.234±0.012(0.024)	
13	1.150	46.5	0.253±0.009(0.024)	
14	1.150	71.0	0.209±0.011(0.022)	
15	1.150	91.0	0.131±0.014(0.018)	
16	1.170	46.0	0.247±0.015(0.027)	
17	1.172	89.0	0.135±0.012(0.017)	
18	1.175	69.5	0.196±0.012(0.021)	
1	1.190	92.6	0.129±0.010(0.015)	
2	1.200	92.1	0.143±0.010(0.016)	
3	1.210	91.7	0.124±0.009(0.014)	
4	1.290	89.7	0.125±0.007(0.013)	
5	1.313	89.4	0.129±0.007(0.014)	Göing *et al.*
6	1.335	89.1	0.142±0.007(0.015)	(Ref. 41)
7	1.353	88.9	0.136±0.007(0.014)	
8	1.371	88.7	0.123±0.008(0.014)	
9	1.387	88.6	0.116±0.007(0.013)	
1	0.970	90.0	0.071±0.004(0.006)	
2	0.970	120.0	0.066±0.003(0.006)	
3	0.979	67.4	0.098±0.004(0.008)	
4	1.003	90.0	0.106±0.004(0.008)	
5	1.020	90.0	0.141±0.006(0.012)	
6	1.024	69.1	0.153±0.006(0.012)	
7	1.060	120.0	0.130±0.005(0.010)	
8	1.060	135.0	0.106±0.008(0.011)	
9	1.063	90.0	0.162±0.006(0.013)	
10	1.065	112.3	0.138±0.007(0.012)	
11	1.100	90.0	0.161±0.006(0.013)	Décamp *et al.*
12	1.160	105.0	0.107±0.005(0.009)	(Ref. 42)
13	1.160	120.0	0.077±0.003(0.006)	
14	1.160	135.0	0.069±0.003(0.006)	
15	1.200	120.0	0.094±0.004(0.008)	
16	1.298	126.5	0.107±0.004(0.008)	
17	1.300	120.0	0.104±0.003(0.008)	
18	1.300	135.0	0.086±0.004(0.007)	
19	1.302	117.2	0.107±0.004(0.008)	
20	1.307	131.7	0.090±0.005(0.008)	
21	1.400	120.0	0.119±0.003(0.009)	
22	1.400	135.0	0.121±0.005(0.010)	
1	1.050	24.0	0.342±0.030(0.036)	
2	1.100	28.0	0.396±0.020(0.031)	Feller *et al.*
3	1.200	30.0	0.353±0.019(0.028)	(Ref. 43)

TABLE X. Differential cross section data for the reaction $p(\gamma,K^+)\Lambda$ reported with statistical errors only. The first column numbers the data points as referred to in Fig. 2.

No.	E_γ^{lab} (GeV)	$\theta_K^{\text{c.m.}}$ (deg)	$d\sigma/d\Omega^{\text{c.m.}}$ (μb/sr)	Reference
1	0.960	90.0	0.118±0.035	
2	1.000	42.0	0.161±0.020	
3	1.000	72.0	0.186±0.028	
4	1.000	90.0	0.146±0.023	Donoho *et al.*
5	1.060	64.0	0.219±0.032	(Ref. 44)
6	1.060	90.0	0.147±0.026	
7	1.060	110.0	0.130±0.032	
1	0.953	35.0	0.115±0.020	
2	1.000	28.5	0.160±0.023	
3	1.000	72.0	0.156±0.018	Brody *et al.*
4	1.000	72.0	0.151±0.012	(Ref. 45)
1	1.160	36.0	0.259±0.017	
2	1.160	60.0	0.206±0.012	
3	1.160	75.0	0.205±0.016	
4	1.160	90.0	0.133±0.010	
5	1.160	135.0	0.079±0.009	
6	1.400	17.5	0.271±0.023	Anderson *et al.*
7	1.400	25.0	0.260±0.020	(Ref. 46)
8	1.400	32.5	0.273±0.020	
9	1.400	40.0	0.244±0.020	
10	1.400	45.0	0.254±0.016	
11	1.400	60.0	0.221±0.012	
12	1.400	75.00	0.183±0.013	
13	1.400	90.0	0.156±0.008	
14	1.400	142.5	0.132±0.019	
1	0.942	60.0	0.067±0.006	
2	0.964	54.0	0.093±0.006	Mori (Ref. 47)

[1]See, e.g., C. B. Dover and G. E. Walker, Phys. Rep. **89**, 1 (1982); R. E. Chrien, Nuovo Cimento **102A**, 727 (1989).

[2]For a recent review, see J. Cohen, Int. J. Mod. Phys. **A4**, 1 (1989).

[3]R. A. Adelseck, C. Bennhold, and L. E. Wright, Phys. Rev. C **32**, 1681 (1985).

[4]R. A. Adelseck and L. E. Wright, Phys. Rev. C **38**, 1965 (1988).

[5]J. J. de Swart, Rev. Mod. Phys. **35**, 916 (1963).

[6]See, e.g., N. M. Queen and G. Violini, *Dispersion Theory in High Energy Physics* (MacMillan, London, 1974).

[7]B. Saghai, Jornées d'Etudes de Physique Nucléaire sur la Photoproduction et Electroproduction de Mésons sur le Nucléon et les Noyaux, Lyon, 1986 (Institut de Physique Nucléaire de Lyon, Report 1986), p. 273.

[8]*Low and Intermediate Energy Kaon-Nucleon Physics,* edited by E. Ferrari and G. Violini (Reidel, Dordrecht, 1981).

[9]A. D. Martin, Nucl. Phys. **B179**, 33 (1981).

[10]J. Antolin, Z. Phys. C **31**, 417 (1986).

[11]M Bozoian, J. C. H. van Doremalen, and H. J. Weber, Phys. Lett. **122B**, 138 (1983).

[12]M. M. Nagels, T. A. Rijken, and J. J de Swart, Phys. Rev. D **15**, 2547 (1977).

[13]H. Thom, Phys. Rev. **151**, 1322 (1966).

[14]F. M. Renard and Y. Renard, Nucl. Phys. **B25**, 490 (1971); Y. Renard, *ibid.* **B40**, 499 (1972).

[15]A. S. Rosenthal, D. Halderson, K. Hodgkinson, and F. Tabakin, Ann. Phys. (N.Y.) **184**, 33 (1988).

[16]C. Bennhold, Phys. Rev. C **39**, 1944 (1989).

[17]J. Cohen, Phys. Rev. C **39**, 2285 (1989).

[18]N. Levy, W. Majerotto, and B. J. Read, Nucl. Phys. **B55**, 493 (1973); **B55**, 513 (1973).

[19]J. Cleymans and F. E. Close, Nucl. Phys. **B85**, 429 (1975).

[20]N. F. Nelipa, Nucl. Phys. **82**, 680 (1966); A. R. Pickering, *ibid.* **B66**, 493 (1973).

[21]W. Schorsch, J. Tietge, and W. Weilnböck, Nucl. Phys. **B25**, 179 (1970).

[22]R. A. Adelseck and B. Saghai, *Session d'Etudes Biennale de Physique Nucléaire,* Aussois, 1989, edited by J. Meyer (Institut de Physique Nucléaire de Lyon, 1989) p. S.1.

[23]J. D. Bjorken and S. D. Dreel, *Relativistic Quantum Mechanics* (McGraw-Hill, New York, 1964).

[24]Particle Data Group, Phys. Lett. B **204**, 1 (1988).

[25]G. F. Chew, M. L. Goldberger, F. E. Low, and Y. Nambu, Phys. Rev. **106**, 1345 (1957).

[26]M. Jacob and G. C. Wick, Ann. Phys. (N.Y.) **7**, 404 (1959).
[27]P. J. Bussey *et al.*, Nucl. Phys. **B154**, 205 (1979).
[28]I. S. Barker, A. Donnachie, and J. K. Storrow, Nucl. Phys. **B95**, 347 (1975).
[29]N. S. Craigie, K. Hidaka, M. Jacob, and F. M. Renard, Phys. Rep. **99**, 69 (1983).
[30]G. R. Goldstein, J. F. Owens III, J. Rutherfoord, and M. J. Moravcsik, Nucl. Phys. **B80**, 164 (1974).
[31]C. R. Ji and S. R. Cotanch, Phys. Rev. C **38**, 2691 (1988).
[32]R. L. Workman and H. W. Fearing, Phys. Rev. D **37**, 3117 (1988).
[33]W. A. Bardeen and E. W. Torigoe, Phys. Rev. C **3**, 1785 (1971).
[34]H. Burkhardt, J. Lowe, and A. S. Rosenthal, Nucl. Phys. **A440**, 653 (1985).
[35]G. Ya. Korenman and V. P. Popov, Phys. Lett. **40B**, 628 (1972).
[36]R. L. Anderson, E. Gabathuler, D. Jones, B. D. McDaniel, and A. J. Sadoff, Phys. Rev. Lett. **9**, 131 (1962).
[37]C. W. Peck, Phys. Rev. **135**, B830 (1964).
[38]D. E. Groom and J. H. Marshall, Phys. Rev. **159**, 1213 (1967).
[39]A. Bleckmann, S. Herda, U. Opara, W. Schulz, W. J. Schwille, and H. Urbahn, Z. Phys. **239**, 1 (1970).
[40]T. Fujii *et al.*, Phys. Rev. D **2**, 439 (1970).
[41]H. Göing, W. Schorsch, J. Tietge, and W. Weilnböck, Nucl. Phys. **B26**, 121 (1971).
[42]D. Décamp, B. Dudelzak, P. Eschstruth, and Th. Fourneron, Orsay Linear Accelerator Report LAL-1236, 1970; Th. Fourneron, Thése de Doctrat d'Etat, Orsay Linear Accelerator Report LAL-1258, 1971.
[43]P. Feller, D. Menze, U. Opara, W. Schulz, and W. J. Schwille, Nucl. Phys. **B39**, 413 (1972).
[44]P. L. Donoho and R. L. Walker, Phys. Rev. **112**, 981 (1958).
[45]H. M. Brody, A. M. Wetherell, and R. L. Walker, Phys. Rev. **119**, 1710 (1960).
[46]R. L. Anderson, E. Gabathuler, D. Jones, B. D. McDaniel, N. B. Mistry, S. Mori, A. J. Sadoff, and N. R. Stanton, in *Proceedings of the International Symposium on Electron and Photon Interactions at High Energies,* Hamburg, 1965, edited by G. Höhler, G. Kramer, and U. Meyer-Berkhout, (Deutsche Physikalische Gesellschaft, 1966), p. 203.
[47]S. Mori, Ph.D. thesis, Cornell University, 1966.
[48]R. Erbe *et al.*, Phys. Rev. **188**, 2060 (1969).
[49]H. Thom, E. Gabathuler, D. Jones, B. D. McDaniel, and W. M. Woodward, Phys. Rev. Lett. **11**, 433 (1963).
[50]B. Borgia, M. Grilli, P. Joos, L. Mezzetti, M. Nigro, E. Schiavuta, and F. Villa, Nuovo Cimento **32**, 218 (1964).
[51]M. Grilli, L. Mezzetti, M. Nigro, and E. Schiavuta, Nuovo Cimento **38**, 1467 (1965).
[52]R. Hass, T. Miczaika, U. Opara, K. Quabach, and W. J. Schwille, Nucl. Phys. **B137**, 261 (1978).
[53]K. H. Althoff *et al.*, Nucl. Phys. **B137**, 269 (1978).
[54]H. Tanabe, M. Kohno, and C. Bennhold, Phys. Rev. C **39**, 741 (1989).
[55]A. M. Bernstein, T. W. Donnelly, and G. N. Epstein, Nucl. Phys. **A358**, 195c (1981).
[56]S. S. Hsiao and S. R. Cotanch, Phys. Rev. C **28**, 1668 (1983).
[57]F. Dydak *et al.*, Nucl. Phys. **B118**, 1 (1977).
[58]P. C. Petersen *et al.*, Phys. Rev. Lett. **57**, 949 (1986).
[59]J. Lowe *et al.*, Nucl. Phys. **B209**, 16 (1982).
[60]B. L. Roberts *et al.*, Nuovo Cimento **102A**, 145 (1989); D. A. Whitehouse *et al.*, Phys. Rev. Lett. **63**, 1352 (1989).
[61]J. Lowe, Nuovo Cimento **102A**, 167 (1989).
[62]W. M. Gibson and B. R. Pollard, *Symmetry Principles in Elementary Particle Physics* (Cambridge University Press, Cambridge, 1976), Chaps. 8 and 10. *Notice a sign misprint in the final expression for the* Σ^0-Λ *transition moment* (p. 306).
[63]O. Dumbrajs, R. Koch, H. Pilkuhn, G. C. Oades, H. Behrens, J. J. de Swart, and P. Kroll, Nucl. Phys. **B216**, 277 (1983).
[64]J. F. Donoghue and B. R. Holstein, Phys. Rev. D **25**, 2015 (1982).
[65]See, e.g., M. D. Scadron, *Advanced Quantum Theory* (Springer-Verlag, New York, 1979), p. 274; J. F. Donoghue and B. R. Holstein, Phys. Rev. D **25**, 206 (1982).
[66]R. A. Adelseck, Saclay Report DPh-N/Saclay 2576 B, 1989.
[67]*Photoproduction of Elementary Particles,* Vol. 8 of *Landolt-Börnstein Numerical Data and Functional Relationships in Science and Technology,* edited by H. Genzel, P. Joos, and W. Pfeil (Springer, New York, 1973), pp. 285–292.